ABSTRACT

CARBON-13 KINETIC ISOTOPE EFFECT IN THE THERMAL ISOMERIZATION OF METHYL ISOCYANIDE

by John Frederick Wettaw

The carbon-13 kinetic isotope effect in the thermal unimolecular isomerization of methyl isocyanide to acetonitrile was investigated from 1 atmosphere to 1 centimeter pressure at 243.4, 226.0, and 213°C.

Methyl isocyanide was prepared from silver cyanide and methyl iodides. Purified methyl isocyanide (labeled with natural abundance ^{13}C in both carbon prositions) was isomerized and the remaining unreacted methyl isocyanide separated by gas chromatography from the product acetonitrile. The fraction of reaction was determined from the ratio of the areas on the chromatogram, and the separated products were trapped and retained for analysis.

The products were oxidized over copper oxide at 600°C and the carbon dioxide separated from the water and nitrogen products and purified by vacuum sublimation. The $^{13}CO_2/^{12}CO_2$ molar ratio R was determined on the carbon-dioxide derived from oxidation of methyl isocyanide (R_{NC}) and acetonitrile (R_{CN}) obtained at fraction f of reaction. The three data R_{NC}, R_{CN}, and f define a C-13 kinetic isotope effect $r = k/k'$, which is an average of the isotope effects $r_1 = k/k_1$ arising from labeling in the methyl carbon position and $r_2 = k/k_2$ arising from labeling at the isonitrile carbon.

At high pressures the average isotope effect r is given by

$$r_{\infty} = 0.998 \exp(20 \pm 5/RT) \quad .$$

At lower pressures, the effect declines as expected for a unimolecular reactions, the values at 1 atmosphere and at 1 centimeter being 1.018_5 and 1.011_5, respectively, at 226^0C.

An expression relating the observed average isotope effect r to the isotope effects r_1 and r_2 was derived, and used to compare the experimental results with theoretical values of r_1 and r_2 derived from the RRKM theory of unimolecular reactions for various models of the activated complex. Good agreement between theory and experiment was obtained for a complex model in which one of the degenerate CNC linear bending vibrational modes of methyl isocyanide becomes the reaction coordinate leading to a ring structure as proposed by Rabinovitch and coworkers. The calculated results are quite sensitive to the vibrational frequency pattern of the complex, and it has been possible to define the complex frequencies within rather narrow limits from an examination of all of the experimental results on methyl isocyanide. The carbon-13 isotope effect suggests that the major changes in frequency pattern in going from the molecule to the complex involves lowering the C-N and N≡C stretching frequencies, in agreement with the results of Rabinovitch, et al. on the fall-off

of the rate constant for isomerization and the deuterium isotope effects. The results indicate substantially larger carbon-13 isotope effect associated with labeling at isonitrile position than with that arising from labeling at the methyl carbon.

CARBON-13 KINETIC ISOTOPE EFFECT IN THE THERMAL ISOMERIZATION OF METHYL ISOCYANIDE

By

John Frederick Wettaw

A THESIS

Submitted to
Michigan State University
in partial fulfillment of the requirements
for the degree of

DOCTOR OF PHILOSOPHY

Department of Chemistry

1967

To My Parents

ACKNOWLEDGMENTS

The author wishes to extend his sincere appreciation to Dr. L. B. Sims for his inspiration and guidance during the course of this investigation.

Appreciation is extended to Dr. P. E. Yankwich of the University of Illinois who made available the Isotope-Ratio Mass Spectrometer. In addition thanks is extended to Mr. Thomas Huang of the University of Illinois for his assistance in helping the author with the operation of the Isotope-Ratio Mass Spectometer.

The author wishes to acknowledge two fellow students Mr. Hans P. E. Sachse and Mr. Richard C. Benson who contributed both knowledge and personality during this investigation.

TABLE OF CONTENTS

LIST OF TABLES

LIST OF FIGURES

I. INTRODUCTION

A gas-phase reaction is described as a unimolecular kinetic process if the formally-defined first-order rate constant exhibits certain characteristics: at high pressures, the rate constant approaches a limiting constant value; as the reactant pressure decreased, the rate constant begins to decline or "fall-off" from the limiting value; and at sufficiently low pressures, the rate constant becomes proportional to reactant concentration, so that the kinetics may be described by a second-order rate law.

Early experiments on unimolecular reactions were limited to the high pressure first-order region. The first-order rate constants were strongly dependent on the temperature, suggesting that the molecule must contain a certain minimum energy approximately equal to the observed activation energy for reaction. The existence of first-order kinetics, however, seems inconsistent with a collisional activation process, since collisional activation is a second-order process. Perrin[1] suggested that dissociation followed absorption of radiation whose frequency was proportional to the activation energy per molecule. The radiation theory was shown to be inconsistent with other aspects of these reactions and was replaced by the Lindemann[2] hypothesis that collisional activation could lead to an observed first-order rate law at high pressures, if the mean lifetime of a high

energy (active) molecule were long compared to the time between collisions. Under these conditions, an effective steady concentration of active molecules would be maintained by collisional activation--deactivation processes, the actual concentration of active molecules (to which the rate is directly proportional) being limited by the concentration of reactant molecules. At sufficiently low pressures, the time between collisions would necessarily be long relative to the lifetime of an active molecule, so that every active molecule would react. The rate in this case would be limited by the collisional activation reaction, a second-order process.

The quantitative explanation of the decline of the first-order rate constant with decreasing pressure requires an extension of the Lindemann hypothesis. The pressure range of the fall-off will depend on the relative magnitudes of the rate of collisional deactivation and spontaneous decomposition of active molecules. All of the theories of unimolecular reactions have incorporated the strong collision assumption[3] of deactivation at every collision, and the rate of collisional deactivation is equated to the kinetic theory collision frequency. The rate of spontaneous decomposition, however, depends on the molecular model for the active molecule and on the criterion for reaction, which are treated differently in the various theories of unimolecular reactions. Classical theories of unimolecular reactions have been

developed principally by Hinshelwood[4], Rice and Rampsberger[5], Kassel[6], (referred to collectively as the RRK theory) and more recently by Slater. Quantum theories have been developed by Kassel[6], Slater [1], and by Marcus and Rice[7,8] (referred to as the RRKM theory).

The development of these theories requires certain basic assumptions that should be tested in accordance with available experimental information. Because of the numerous technical difficulties encountered in the observation of gaseous unimolecular reactions, reliable experimental data have been lacking until fairly recently. A number of gaseous reactions which once were believed to be unimolecular have now been shown to have complex mechanisms. The mechanisms of certain complex reactions, such as the decomposition of N_2O_5, [9,10] may include a unimolecular elementary step whose rate can be determined under special conditions. Despite the uncertainty as to the proper characterization of many reactions, there are a number of reactions which have been studied in sufficient detail to determine unambiguously that the reaction occurs as a unimolecular process. In addition to the decomposition of N_2O_5, the best-documented [11] examples of gas-phase unimolecular reactions include the structural isomerization of cyclopropane,[12,13] cyclobutane,[14] and many other substituted cyclopropanes and cyclobutanes, and more recently the isomerization of methyl isocyanide.[15,16]

Kinetic isotope effects have recently been used extensively to study details of the mechanisms of unimolecular

comparison of theory with experiment are simple and more meaningful. Useful information concerning the validity of the strong collision assumption, relative collisional efficiences for energy exchange, and other assumptions of the theories may be obtained from such comparisons if the reaction mechanism is sufficiently well-characterized.

The detailed fall-off behavior[15] of the rate constant, and the deuterium isotope effect [16] in the isomerization of methyl isocyanide have been investigated by Schneider and Rabinovitch. Good agreement of the RRKM calculated results with experiment have been obtained[21] for a complex model in which one of the degenerate CNC bending modes becomes the reaction coordinate. The C-N and N≡C molecule frequencies were lowered in the complex to improve agreement with experiment, and other molecule frequencies were assumed unchanged in the complexes. However, the calculated fall-off behavior and the deuterium isotope effect are not very sensitive to the details of the complex vibrational frequency pattern, especially since the deuterium isotope effect is a secondary isotope effect in this reaction. More direct and detailed information on the vibrational frequency pattern of the complex might be obtainable from the carbon-13 isotope effect. At least the carbon-13 isotope effect would be excellent confirmatory evidence for the suggested detailed mechanism.

II. HISTORICAL

A. THEORIES OF UNIMOLECULAR REACTIONS

1. Generalized Formulation of the Apparent First-Order Rate Constant

The development of the theory of reaction rates has its beginning in the proposal by Arrhenius[22] that the very strong temperature dependence of the rate constant for the inversion of sucrose was given by the equation:

$$k = A \exp(-E_a/RT) \qquad (1)$$

where the constants A and E_a are the pre-exponential factor and the experimental activation energy, respectively. This temperature dependence was interpreted to mean that molecules can react only from certain special states characterized by high energy. Molecules in these special states lying above a minimum citical energy E_c necessary for reaction are termed "active". The temperature dependence of most rate constants is given adequately by an Arrhenius expression.

Let $i = 1,2,3,$ ----- be an enumeration of these states. These states may be continuous or, quantized and may be specified by one or more parameters but a different notation for classical and quantum models is not necessary to the present development. If a fraction f_i of molecules are in state i, from which the probability of reaction is c_i per unit time, the observed first-order rate constant is

$$k = \sum_i c_i f_i \qquad (2)$$

where the summation is over all states i of the active molecules.

The distribution function f_i may differ markedly depending upon the method of excitation used. Experimental techniques other than collisional activation or "thermal" methods include chemical activation, photosensitization and electron impact. The specific decomposition rate of active molecules c_i depends only upon the properties of the active molecules once formed.

2. Distribution Function for Active Molecules in a Thermal System. The Lindemann Mechanism.

The Lindemann hypothesis [2] of a time lag between the collision-energization and the dissociation of active molecules is represented for a thermal reaction

$$A \xrightarrow{k} \text{Products}$$

by the following collision mechanism[23]

$$\begin{aligned} A + M &\xrightarrow{a_i} A_i^* + M \\ A_i^* + M &\xrightarrow{b_i} A + M \\ A_i^* &\xrightarrow{c_i} \text{Products} \end{aligned} \qquad (3)$$

where A represents the reacting species, M being any species with which A can collide and exchange energy, A_i^* a molecule of species A which has been activated to level

i, a_i, b_i, c_i the rate constants for collisional activation, collisional deactivation, and spontaneous decomposition of the active molecule in level i, respectively, and k is the observed overall rate constant.

At high pressures, the molecular distribution among the allowed energy levels will be essentially the statistical equilibrium distribution of a non-reacting gas. At lower pressures, the concentration of active molecules will be reduced by reaction and the fraction of molecules in any level i can be found by application of the steady-state approximation to the concentration of the species A_i^*:

$$-\frac{dA}{dt} \equiv 0 = a_i(A)(M) - b_i(A_i^*)(M) - c_i A_i^*$$

which leads to

$$(A_i^*) = \frac{a_i(A)(M)}{c_i + b_i(M)} \qquad (4)$$

The fraction of molecules in state i is therefore

$$f_i = \frac{A_i^*}{A_i} = \frac{(a_i/b_i)\, b_i(M)}{b_i(M) + c_i} \qquad (5)$$

where a_i/b_i is the equilibrium fraction, F_i, of active molecules A_i^* in a non-reacting gas.

Invoking the strong collision assumption [1], that collisional deactivation efficiency is unity for all levels i, leads to the expression

$$b_i(M) = ZP = \omega \qquad (6)$$

where ω is the kinetic theory collision frequency at

pressure P, Z being the collision probability per unit time per unit pressure.

The observed overall rate constant k thus may be expressed in the following form

$$k = \sum_i \frac{c_i F_i \omega}{\omega + c_i} \qquad (7)$$

The fraction of active molecules A_i^* in a non-reacting gas, F_i, can be calculated from the Boltzman equation[24] and the molecular model The rate constant for spontaneous decomposition of A_i^*, c_i, likewise depends on the molecular model and, in addition, on the assumed criterion for reaction, both of which are treated differently in the various theories of unimolecular reactions.

3. Early Classical Theories

Lindemann's hypothesis was first developed mathematically by Hinshelwood in 1926.[4] The theory is based on the assumption that the rate constant for spontaneous decomposition is independent of the amount of energy in excess of the critical minimum; i.e., $c_i = c$ for all i, where c is an average specific decomposition rate.

Comparison of the Hinshelwood theory with experimental data results in very poor agreement. Clearly the assumption that active molecules have the same rate constant for spontaneous decomposition from all levels i is an over-simplification. A more reasonable assumption, that the lifetime

of an active molecule is a function of the energy in excess of the critical minimum, has been incorporated into more recent theories of unimolecular reactions, both classical and quantum mechanical.

The classical theories of Kassel[6] and of Rice and Rampsberger [5] are essentially identical, in that the model of the reactant molecule is that of a set of lightly coupled classical harmonic oscillators. The molecule reacts whenever the requisite amount of energy , E_i, greater than E_c, accumulates in an critical oscillator.

The rate constant for spontaneous decomposition is assumed from statistical arguments to be of the form

$$c_i = 0 \qquad \text{for} \quad E_i \leq E_c$$

$$c_i = A \left[\frac{E_i - E_c}{E_i} \right]^{s-1} \qquad \text{for} \quad E_i > E_c$$

where A is identified with the high pressure pre-exponential Arrhenius factors and s is the number of effective oscillators (those which contribute their vibrational energy to the observed activation energy) of the molecule. The value of s is chosen to give the best agreement between calculated and experimental decline of the fall-off of the rate constant with pressure. The basic assumption of classical harmonic oscillators for representation of molecular vibrations and the fact that s has the status of an adjustable curve-fitting parameter, which must be allowed to assume physically unreasonable non-integral values in order

to obtain agreement between theory and experiment, are the most serious short comings of the theory. In addition the oscillators are not clearly defined.

4. The Slater Theory Classical

Slater [25] takes as the model for the reacting molecule, a vibrating system of n non-interacting classical oscillators at all energies. The oscillators change energy content only during a collision with other molecules. The oscillators are identified in Slater theory with the classical normal mode oscillators of vibration theory. The internal displacement coordinates q_i, of the molecule are then linear combinations of the normal displacement coordinates Q_j. Reaction is assumed to occur when a "critical" internal distance (coordinate) attains a critical extension in the direction necessary for reaction. This will occur whenever the normal modes of vibration come sufficiently into phase.

The rate constant for spontaneous decomposition then has the form:

$$c_i = \nu \left[\frac{E - E_c}{E}\right]^{1/2n}$$

where E is total vibrational energy, distributed in all possible ways among the various oscillators; n, the number of non-degenerate frequencies, determined by the symmetry properties of the molecule; and ν, a weighted average of the n vibrational frequencies.

While the Slater theory is more appealing because there are no parameters which are not determined by properties of the reacting active molecule, comparisons with experiment indicate gross errors, particularly with regard to the assumption of uncoupled oscillators, which precludes intramolecular energy transfer between collisions.[26,27,28,29]

5. The Quantum Statistical Theory of Unimolecular Reactions (RRKM Theory)

The quantum versions of the theories of Kassel and Slater both assume an unrealistic molecular model consisting of harmonic oscillators with degenerate or commensurable frequencies. The RRKM theory [8,9] allows for distinct frequencies of the oscillators. Since the present work is mainly concerned with the RRKM formulation, it will be discussed in more detail than the other theories described.

As was the case in the previous theories, the active molecule is assumed to be harmonic at all energies, but now any or all vibrational degrees of freedom and/or internal rotations may be described as "active", i.e., they contribute their energy to the reaction coordinate. Overall rotations are assumed to be "adiabatic", in the sense that they remain in the same quantum state throughout the reaction, and contribute only centrifugal energy to the reaction. In addition to the minimum energy requirement for reaction, the RRKM theory requires the formation of some specific internal configuration, and is in this respect similar to the transition state theory.[30] The collisional Lindemann mechanism is

modified as follows:

$$A + M \underset{b_i}{\overset{a_i}{\rightleftarrows}} A_i^* + M$$

$$A_i^* \xrightarrow{k_i} A_j^+$$

$$A_j^+ \xrightarrow{\text{fast}} \text{Products}$$

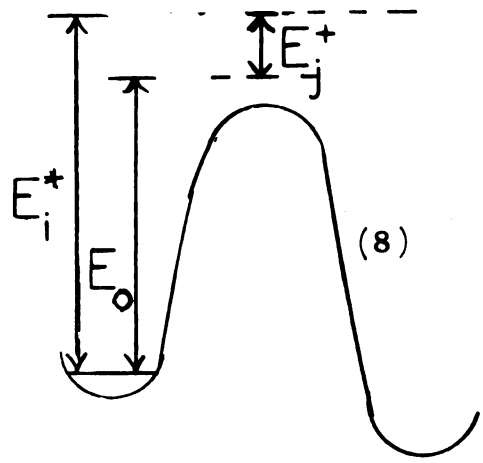

(8)

where A_i^* and A_j^+ represent the active molecule and the "activated complex" with internal energies E_i^* and E_j^+ and k_i represents the probability for formation of a reaction complex from an active molecule at the same total energy in excess of the zero point vibrational energy.

The observed first-order specific rate constant k for the overall reaction

$$A \xrightarrow{\quad k \quad} P$$

is obtained by application of the steady state approximation to A_i^* and A_j^+ in the reaction sequence 8 , which leads to

$$f_i = \frac{a_i/b_i}{1 + \dfrac{k_i}{b_i(M)}} \tag{9}$$

The resulting expression for k (see equation 2) is then

$$k = \sum_i \frac{(a_i/b_i)\, k_i}{1 + \dfrac{k_i}{b_i(M)}} \tag{10}$$

where i represents all energy states of the active molecule.

Development of a final expression for k in terms of molecular parameters, depends upon whether the activated complex is "rigid" (if only vibrational degrees of freedom are considered active), or "loose" (if internal rotations are also active). In the present work only rigid complexes are considered.

The summation in equation 10 is appropriate for a quantized model, but may be replaced by an integral over internal energy for thermal systems for the following reasons: In the case of the active molecule at energies in excess of the critical energy (several Kcal/mole), the vibrational energy states are extremely dense, so that a continuous density function may be used with confidence; in the formation of the complex, one of the real vibrational degrees of freedom of the active molecule becomes an internal translational degree of freedom along the reaction coordinate. The quantized nature of the complex vibrations is quite apparent at the relatively low energies (relative to the zero-point vibrational energy of the complex) involved, and cannot be treated as continuous; however, as any distribution of the internal energy of the complex between real vibrational modes and the internal translational mode is possible, so long as consistent with the quantized nature of the vibrations, the energy E^+ of the complex will be continuous.

The term a_i/b_i in equation 10 then becomes $F(E^*)dE^*$, the equilibrium fraction of active molecules at energy E^*

to $E^* + dE^*$, given by [24]

$$F(E^*)dE^* = \frac{N^*(E^*)\ \exp(-E^*/kT)\ dE^*}{Q_v^*} \quad , \qquad (11)$$

where $N^*(E^*)$ is the density of active energy states at E^*, and Q_v^* is the vibrational partition function for the active molecule.

The term $b_i(M)$ in equation 10 is set equal to the collision frequency ZP at all energies (strong collision assumption).

The specific decomposition rate k_i becomes k_E the decomposition probability for active molecules at energy E^*. k_E represents the probability of forming an activated complex from an active molecule at constant energy; thus k_E will be proportional to the ratio of the number of energy states of the complex at energy E^+ to the number of active vibrational energy states at E^*. The final expression is[33]

$$k_E = \alpha \frac{I_r}{h} \frac{\sum_{E_v^+ \leq E^+} P(E_v^+)}{N^*(E^*)} \qquad (12)$$

where I_r is the inertial ratio, or the ratio of rotational partition functions for the complex to that of the active molecule (this term corrects for the contribution of centrifugal energy of the adiabatic rotations), $P(E_v^{\mp})$ is the vibrational degeneracy at energy E_v^*, and the summation recognizes that any fraction of the total energy E^+ of the complex may be in vibrational degrees of freedom as E_v^*,

(consistent with the quantized nature of the vibrations), the rest being in the internal translational degree of freedom. α is the reaction path multiplicity, a correction factor to account for the possibility that more than one unique path for reaction may exist due to symmetry properties of the molecule. The correct prescription for α will be given in the discussion section.

The final expression for the unimolecular rate constant k for the case of "rigid" complexes becomes:[31]

$$k = \alpha \frac{kT}{h} I_r e^{-E_c/RT} \int_{E^+=0}^{\infty} \frac{\sum_{E_v^+ \leq E^+} P(E_v^+) e^{-E^+/RT}}{1 + \frac{k_E}{ZP}} \frac{dE^*}{RT} \quad (13)$$

At high pressures, equation 13 becomes

$$k_\infty = \alpha \frac{kT}{h} I_r \frac{Q_v^+}{Q_v^*} e^{-E_c/RT} , \quad (14)$$

identical with the transition state expression.[30] At low pressures, the limiting second order rate constant is given by:

$$k_0 = \frac{Z}{Q_v^*} \int_{E_c}^{\infty} N^*(E^*) e^{-E^*/RT} dE^* \quad (15)$$

since $E^* = E_c + E^+$. At low pressures, all dependence on the activated complex disappears.

The critical energy E_c (the difference in zero-point energies of the complex and active molecules) can be related to the experimental activation energy by requiring

the high pressure rate constant (equation 14) to have the experimental temperature dependence. This results in[7,31]

$$E_c = E_a + \langle E_v^* \rangle - \langle E_v^+ \rangle - RT \qquad (16)$$

where $\langle E_v \rangle$ represents average vibrational energy.

6. Kinetic Isotope Effects and Quantum Statistical Effects. (RRKM Theory)

The reaction rates for isotopic molecules, i.e., molecules differing only in the substitution of one or more atoms by isotopes, will generally differ, the effect being referred to as kinetic isotope effect. The fact that the potential energy surfaces of isotopic molecules are very nearly identical[30] , infers that any mechanistic isotope effect will result largely from the mass effect on the vibrational patterns of the isotopic molecules and complexes. Kinetic isotope effects may be described as primary or secondary, depending upon the proximity of the isotopic substitution site to the reaction site. If the atom is intimately involved in the reaction coordinate, the effect is termed primary, while an atom situated at a position relatively removed from the site of the reaction will produce a secondary effect due to the dependence of the reaction coordinate on all of the normal coordinates.

The RRKM theory predicts a decrease in the magnitude of the isotope effect from the high to low pressure region, as do the classical theories.[32] This mechanistic effect results because of the insensitivity of the rate-determining

collisional energization reaction in the low pressure region to isotopic substitution. In addition, the RRKM theory admits of the possibility of other non-mechanistic effects (quantum statistical effects). Consider the ezperssions for the limiting high and low pressure isotope effects:

$$\frac{k}{k'}_{\infty} = \left(\frac{I_r}{I'_r}\right)\left(\frac{Q_v^+}{Q_v'^+}\right)\left(\frac{Q_v^{*\prime}}{Q_v^*}\right) \exp\left(\Delta E_c/RT\right) \qquad (17)$$

$$\frac{k}{k'}_{0} = \frac{Z}{Z'} \frac{\int_{E_0}^{\infty} N^*(E^*)\exp(-E^*/RT)\frac{dE^*}{Q_v^*}}{\int_{E_0}^{\infty} N^*(E^*)\exp(-E^*/RT)\frac{dE^*}{(Q_v^*)'}} \qquad (18)$$

where the prime represents the heavier molecule. In the product of the first three terms is generally only slightly smaller than unity, whereas $\Delta E_c \equiv (E'_c - E_c)$ may be as large as one-two kilocalories, the exponential term always outweighs the first three terms with the result that the isotope effect is "normal" (i.e., $k_{light}/k_{heavy} > 1$).

In 18 , it can be seen that the isotope effect will be strongly dependent upon the ratio of the density of energy states of the two isotopic molecules. This density is much larger for the heavier isotopic molecule at all energies due to the closer spacing of energy levels for a harmonic oscillator of larger mass. Thus an inverse isotope effect should be observed at low pressures. Statistical

weight inverse isotope effects have been observed for both the structural isomerization of cyclopropane[33,39] and the thermal isomerization of methyl isocyanide.[15,16]

3. The Unimolecular Isomerization of Methyl Isocyanide Molecules

The first investigation of the isomerization of the isocyanides was that reported by Ogg.[34] The work was incomplete, but preliminary data on methyl and ethyl isocyanides indicated activation energies of approximately 40 kcal/mole and frequency factor > 10^{13} sec^{-1}. Such data were interpreted as indicating that the reactions were probably unimolecular.

In an exploratory study, an examination of the thermal isomerization of p-tolyl isocyanide was made by Kohlmaier and Rabinovitch.[35] Frequency factors of $10^{13.7}$ sec^{-1} for solution studies and $10^{12.5}$ for gas phase studies were observed, a value $y \sim 10^{13}$ sec^{-1} is characteristic of unimolecular processes. Activation energies of 36.9 kcal/mole and 33.8 kcal/mole for solution and gas phase reactions, respectively, were determined.

The structure of the isocyanides has been shown to involve a linear C-N≡C: submolecule. The degenerate bending motions increase the importance of the valence bond structure $C\text{-}\ddot{N}=C:$, and the isomerization can formally be considered as due to bending of the CNC linear portion of the molecule to form an activated complex in which the carbon

attached to the isonitrile group and the isonitrile carbon can approach one another, facilitating the isomerization to the CCN nitrile structure. In the p-tolyl case, activated complex models involving (a) free rotation about the C-N bond in the complex, and (b) a rigid ring structure, were considered, and it was shown that the ring structure was more consistent with the fairly large entropy of activation (-4.8 e.u.) observed.

The thermal unimolecular isomerization of methyl isocyanide to acetonitrile has been investigated by Schneider and Rabinovitch[15] as part of a thorough investigation of this reaction type. Results show the reaction to be a first-order homogeneous reaction in the temperature range 200-260°C. "Fall-off" was studied over a pressure range from several atmospheres to about 0.02 mm, well into the "second-order" region. The activation energy was found to decline with pressure by about two kilocalories between the high-pressure and low-pressure regions. At high pressures, the temperature dependence of the rate constant is given by

$$\log_{10} k = 13.6 - 38{,}350/2.303RT.$$

The RRKM theory was used to calculate the rate constant at a function of pressure, assuming a ring structure for the activated complex, with one of the degenerate CNC modes representing the reaction coordinate. Several vibrational frequency patterns for the complex were considered, but only two gave results reasonably in accord with experiment. In

both, one of the CNC bending frequencies of the molecule was considered to become internal translational motion in the complex, and was removed. In the 300 model of Schneider and Rabinovitch, the C-N and N≡C stretching frequencies were lowered slightly, and all other molecule frequencies were considered as unchanged in the complex. In the 700 model, in addition the frequency changes in the 300 model, the second CNC molecule bending frequency was assumed to increase from 300 to 700 cm^{-1} in going to the complex. The agreement with experiment was slightly better for the 300 model, but the calculated results were fairly insensitive to changes in the vibrational frequency pattern of the complex.

The deuterium kinetic isotope effect ($k(CH_3NC)/k(CD_3/NC)$ or k_H/k_D) has also been investigated by Schneider and Rabinovitch. A large statistical weight inverse isotope effect ($(k_H/k_D)_0 = 0.28$) was observed at low pressures, as predicted by the RRKM theory. The deuterium isotope effect is a secondary isotope effect in the isomerization, as reflected by the small limiting high pressure value observed, $(k_H/k_D)_\infty = 1.07$. The calculated RRKM values using the 300 model are 0.38 and 1.35, respectively, in fair agreement with experiment. Better agreement has recently been obtained by Rabinovitch and co-workers [21] using a 300-type model in which the lowering of the molecule C-N and C≡N stretching frequencies were smaller in going to the complex than in the original 300 model, and an improved frequency

assignment for the molecule was used. The RRKM calculated values for the improved model are reported as $(k_H/k_D)_0$= 0.315 and $(k_H/k_D)_\infty$ = 1.21, in better agreement with experiment. The relative efficiencies for collisional energy exhange were determined for a large number of unreactive gases added to the low pressure region in order to assess the validity of the strong collision assumption. The results indicate that the assumption is excellent except for very small molecules (diatomics and triatomics, where it is still a reasonably good approximation), and monatomic gases such as the rare gases.

III. EXPERIMENTAL

A. MATERIALS

1. Helium (Matheson Co., High Purity) was used without purification as the carrier gas in all gas chromatogrpahy work.
2. Ethane (Matheson Co., C. P. Grade) was passed directly from a cylinder, through a dry-ice-alcohol trap, into a storage bulb on the vacuum system. Further purification was effected by numerous trap-trap vacuum distillations before being used in inert-gas runs.
3. Acetonitrile (Fisher Certified Reagent) was purified by distillation in vacuum before use in gas chromatography studies.
4. Methyl Isocyanide was prepared by the method described by Schneider[36], which is a modification of a widely-used method due to Gautier[37]. This method was found to give good yields and a product which did not require extensive purification.

In a typical preparation 0.16 mole of powdered AgCN (Fisher Purified used without further purification) were placed in a cylinderical Pyrex reaction vessel (3.8 cm id. and 10 cm long) which had a seal-off attached to one end. This reaction vessel was attached to vacuum line via 10/30

standard taper joined to the seal-off end of the vessel. The vessel was evacuated and 0.08 mole (5.0 cc) of CH_3I (Baker white label, used without further purification) were distilled on top of the AgCN. The vessel was sealed off and the mixture of CH_3I and AgCN allowed to warm to room temperature. The vessel was clampled to the arm of an electric shaker which extended into a water bath whose temperature was maintained between 55 and 60°C. At this temperature the pressure of CH_3I in the reaction vessel approaches two atmospheres so the bath and shaker were shielded with a glass window. After about an hour and a half the contents of the reaction vessel turned a light yellow color. Termination of the reaction at this point prevented the formation of hard brown polymer products which cut down the yield considerably.

The sealed tube was broken, the contents of which were then powdered and poured into a 100 cc round bottom flask fitted with a 24/40 standard taper joint. After addition of 50 cc of a concentrated KCN solution, (prepared from Baker analyzed KCN) the flask was attached to a vacuum line by use of a 24/40 -10/30 standard taper adapter. The solution was quickly cooled to liquid nitrogen temperature and evacuated. All air was removed by the pump-freeze-melt technique.

The mixture was allowed to warm up to 0°C and the CH_3NC which was present as an oily layer was vacuum distilled into a sample bulb. Five trap to trap distillations from an ice-salt bath at -20°C removed all traces of water.

The resulting sample was checked on a carbowax 20M gas chromotagraphic column for impurities. The only impurity found was CH_3I, and that in very small amounts never exceeding 0.3 mole %.

B. APPARATUS

1. Furnace

The furnace consisted of two concentric heating elements as shown in the schematic of the furnace assembly Figure 1. The inner heating element consisted of three heater sections wound on a steel cylinder (4130 grade alloy steel, five inches in diameter, twenty inches in length, closed on bottom with a 1/4 inch bolt-on steel plate). Five layers of asbestos paper, then three thirty-foot sections of Chromel-A heating wire (B & S #22 gauge, 0.997 ohms/foot), were wound around the inner cylinder. The inner heating element was completed by covering the heating wire as well as the bottom plate with ten layers of asbestos paper. The three heater sections were powered by three manually-controlled 7.5 amp Variacs capable of dissipating 400 watts power each at 110 volts.

The outer heating element consisted of two heater sections wound on a steel cylinder (4130 grade Alloy steel, seven inches in diameter, twenty-six inches in length, closed on the bottom with a 1/4 inch bolt-on steel plate). Each of these two heater sections consisted of parallel windings of two sixty-foot lengths of Chromel-A heating wire (B & S

Figure 1.

Schematic of Furnace Assembly

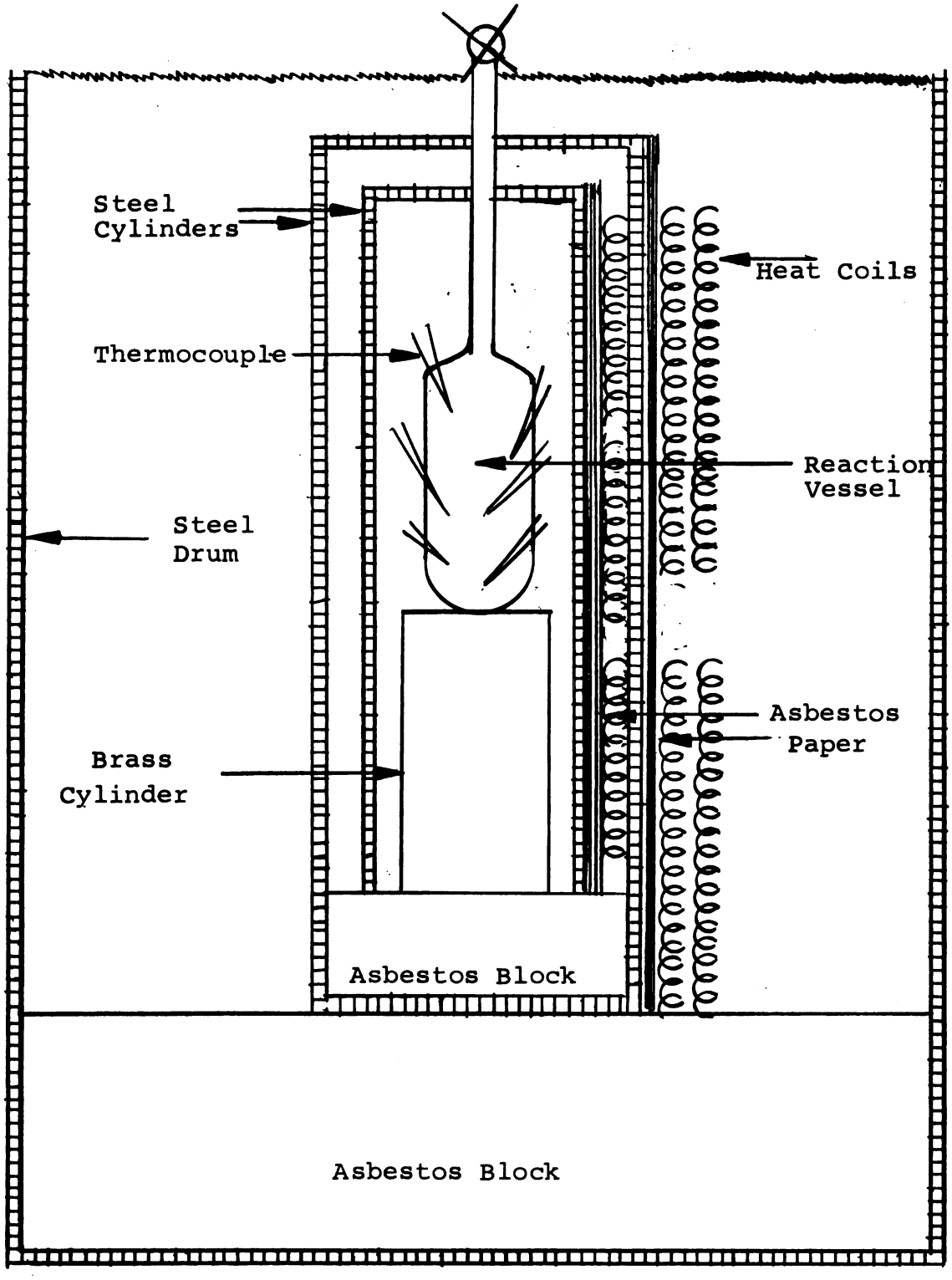
Steel
Cylinders
Heat Coils
Thermocouple
Reaction
Vessel
Steel
Drum
Asbestos
Paper
Brass
Cylinder
Asbestos Block
Asbestos Block

Figure 1.

#22 gauge, 0.403 ohm/foot). The outer heating element was then completed by covering the heating wires as well as the bottom plate with ten layers of asbestos paper. These two sections, which comprised the main heater, were capable of dissipating 1000 watts each at 100 volts, and were powered by 15 amp manually-controlled Variacs.

The furnace was assembled by placing the inner cylindrical heating element on asbestos blocks inside the outer cylindrical heating element, which in turn was set on asbestos blocks inside a fifty-five gallon steel drum. Both heating elements were closed at the top with 1/4 inch bolt-on steel plates, each of which had two one-inch slots at 90^0 to each other cut radially nearly to the center to allow thermocouples, reaction flask neck, etc., to extend from the furnace. The space between the steel drum and the outer heater was filled with Vermiculite (mica) insulation. The reaction vessel rested on an asbestos-covered section of five inch brass tubing placed inside the inner heater, so that the reaction vessel occupied the central third of the vertical space, and its neck was then connected to the vacuum system by means of a 6 mm stopcock directly above the assembled furnace. The thermocouple leads and the leads to the section heaters were brought out through the upper steel plates, and the top of the assembly was covered with Vermiculite insulation. When the furnace assembly was complete the layer of Vermiculite surrounding the outer heating element was about three inches thick.

2. Temperature Regulation System

The reaction vessel was heated by radiation from the inner wall of the inner heating element, which was about one-half inch from the surface of the vessel. The main source of heat was the outer heating element, approximately three inches from the reaction vessel. The temperature was maintained to within 10 - 20^{0}C of the desired reaction temperature by manually adjusting the two 15 amp Variacs to the main heater. A Stabiline 3 KVA line voltage regulator was interposed between the 100 V source and the Variacs. Fine adjustment to attain the required reaction temperature was made by adjustment of the three 7.5 amp Variacs which powered the three inner heating elements. Since these Variacs were normally set to a small percentage of their voltage output, changes in the line voltage did not change the temperature of the reaction vessel appreciably.

The regulation system provided a temperature constant and uniform over the entire extent of the reaction vessel to ± 0.1^{0}C for a period of several hours at the reaction temperatures used.

3. Reaction Vessel

The reactor was a cylindrical vessel, 23.9 cm in length and 8 cm inside diameter, (1020 cc) constructed of Pyrex medium-wall tubing. Five Chromel-Alumel and one Platinum-Platinum, 10% Rhodium thermocouples were tied at various positions on the surface of the reactor with asbestos twine.

The neck of the reaction vessel was 10 mm Pyrex medium-wall tubing and was connected to the vacuum system via 6 mm high-pressure stopcock (a solid-bore vacuum stopcock fitted with a Universal stopcock-adapter (Sargent, S-77353). High-pressure stopcocks will be referred to in later section by use of the Symbol PS; high-vacuum stopcocks are indicated by the symbol S).

4. The Furnace Inlet System

The manifold was of conventional design, consisting of a large (20 mm) glass tube MA, Figure 2 to which other sections were attached by means of high-vacuum stopcocks.

The manifold was evacuated by a fore pump, FP (Cenco Hy-Vac 14), connected to the manifold via a 15 mm 3-way stopcock S1 and a liquid-nitrogen cooled trap T1. An oil diffusion pump, D (Consolidated Vacuum Corporation, Model VMF-20), could be introduced between trap T1 and the fore pump FP by means of stopcocks S1 and S2.

The pressure in the manifold was monitored with a thermocouple ionization vacuum gauge, TG1 (Consolidated Vacuum Corporation, Model GIC-110A). Under normal operating conditions, the fore pump was found to be capable of producing a vacuum of at least 0.5 microns. Use of the oil diffusion pump resulted in an ultimate vacuum of better than 0.01 microns in the manifold.

Figure 2.

Schematic of the Furnace Inlet System.

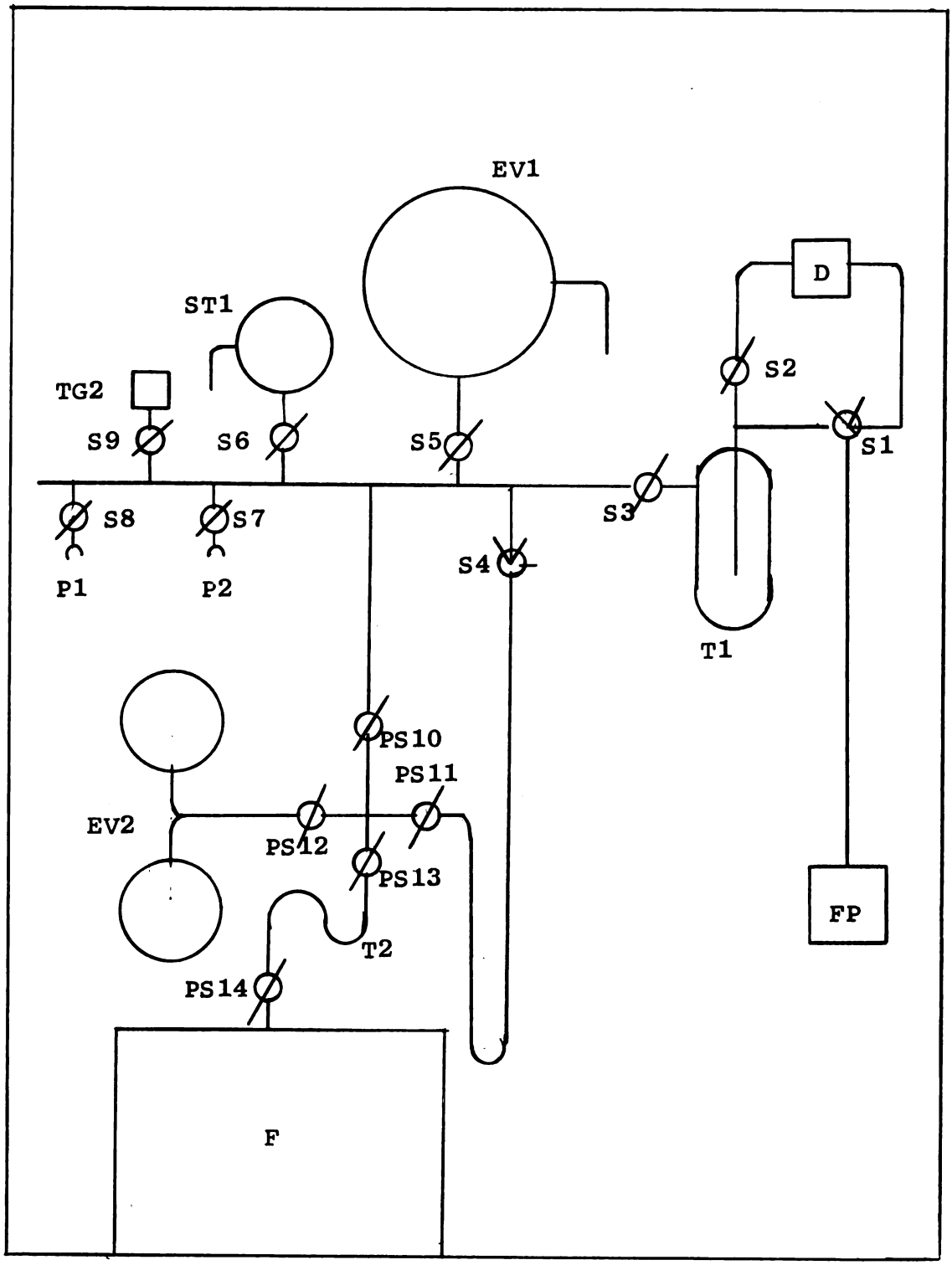
EV1
ST1
D
TG2
S2
S9
S6
S5
S1
S8
S7
S3
P1
P2
S4
T1
PS10
PS11
EV2
PS12
PS13
FP
T2
PS14
F

Figure 2.

5. The Gas Chromatographic Sampling and Collection System

The products of the reaction, acetonitrile and unreacted methyl isocyanide, were separated by gas chromatography. A schematic of the vacuum system is shown in Figure 3 . Sample was introduced from a storage bulb through port P1 into a small (5 cc) trap, T2. Generally about 10 cm pressure, as indicated on the capillary manometer M1, was introduced.

Helium from a cylinder, HE, was used as the carrier gas. The helium stream was plit at x, part being diverted through a reference column RC to the reference side of the detector cell (DC). The remainder of the helium stream either by passed trap T2 containing the sample and flowed directly through the separative column SC, or passed through stopcocks PS5 and PS6, sweeping the sample through SC, the detector cell, the sample collection traps (T3 for methyl isocyanide and T4 for acetonitrile, both cooled to liquid nitrogen temperatures) and finally into the atmosphere through a calibrated ball-type flowmeter, FM. A flow rate of 100 cc/minute generally was used. Usually the products from five sample introductions were combined for mass spectral analysis.

6. The Gas Chromatograph

The design of the gas chromatograph is a modification of that described by L. B. Sims[38]. Full scale deflection of the recorder was produced with less than 10^{-5} mole of

Figure 3. Schematic for the Gas Chromatographic Analysis and Collection System.

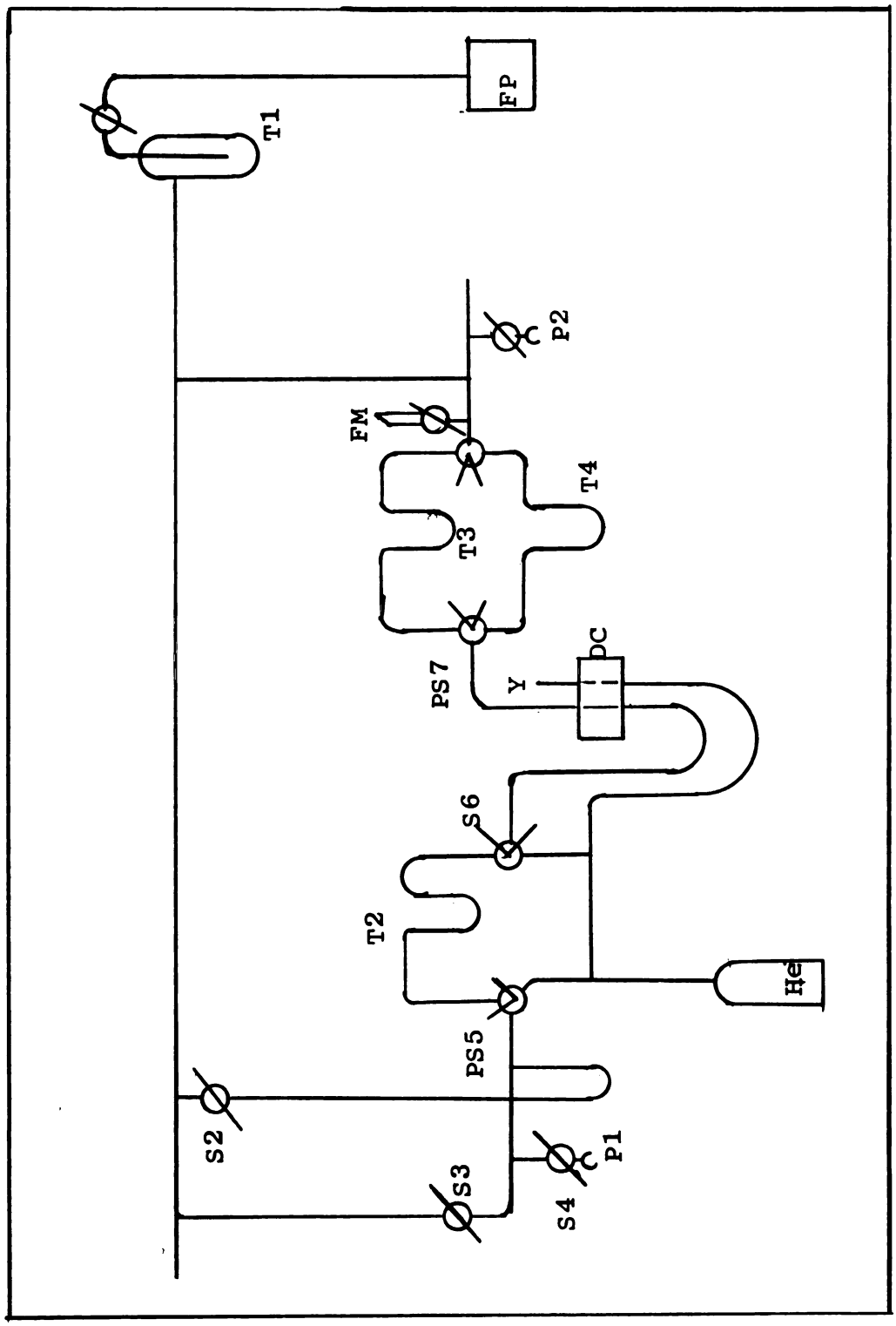

Figure 3.

sample on the most sensitive scale, sufficient to detect impurities of the order of 0.1 mole per cent in the samples.

The chromatograph consisted essentially of four sections: the column, the detector cell, the bridge circuit, and the recorder.

a. The column was 15 ft x 1/4 inch i.d. stainless steel fitted with brass Swagelock connectors and packed with 15% carbowax 20M on 60/80 chromosorb W (Wilkens Instrument Company).

b. The detector cell was a thermal-conductivity cell machined from brass Figure 4. The sensing elements were matched thermistors (Victory Engineering Corporation, type A33), fitted on a Teflon washer on a seat in the detector block, and held in place by means of a threaded brass washer assembly, as shown in Figure 4.

The detector block was connected to the column assemblies suspended in a constant-temperature air furnace beneath by means of Swagelock metal-glass connectors fitted with Teflon ferrules. The sample was swept with helium from the sampling inlet system, through the collection system where the sample was removed from the helium stream. The helium then passed through the flowmeter and issued into the atmosphere.

Figure 4.

Schematic for Gas Chromatographic Detector Block

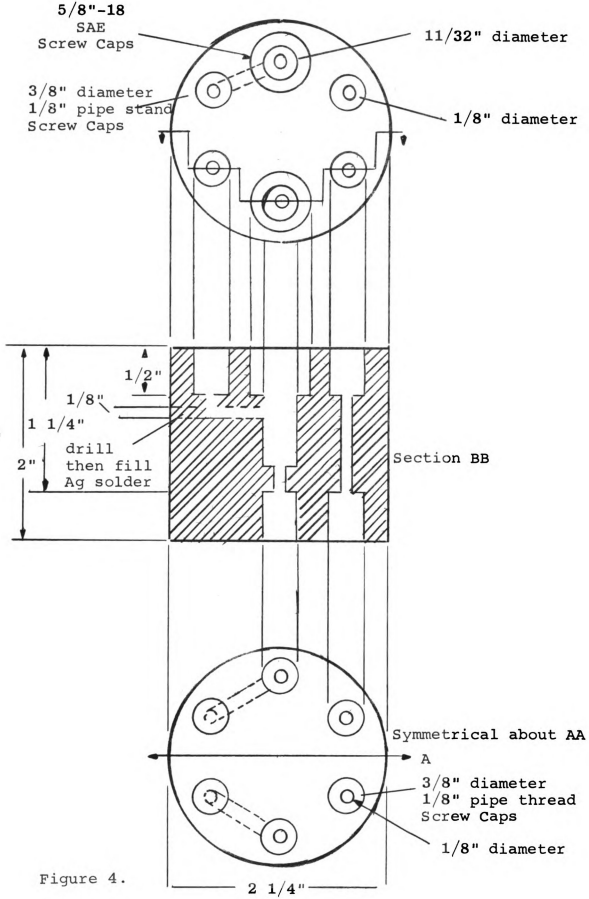
5/8"-18
SAE
Screw Caps
11/32" diameter
3/8" diameter
1/8" pipe stand
Screw Caps
1/8" diameter
1/2"
1/8"
1 1/4"
2"
drill
then fill
Ag solder
Section BB
Symmetrical about AA
A
3/8" diameter
1/8" pipe thread
Screw Caps
1/8" diameter
2 1/4"

Figure 4.

c. A Wheatstone bridge circuit was used to convert the change in resistance of the sensing thermistor, when the gas stream consisted of a "peak" of different thermal-conductivity from the carrier gas, to a change in voltage which was then fed to a recorder. The circuit is shown in Figure 5.

A six-volt P6 storage cell was used as the battern in the circuit. The potential applied to the bridge circuit was set at four volts by the 500 ohm variable resistor R5. The attenuator was set to give nearly full scale deflection (1 mV) on the recorder. The peak areas corresponding to methyl isocyanide and acetonitrile on the chromatograph were measured with a compensating polar planimeter. The ratio of areas methyl isocyanide/acetonitrile was used to determine the fraction f of reaction.

d. The recorder was a Sargent Model SR, variable range. The most sensitive range, 1 millivolt, was used both when analyzing a sample of methyl isocyanide for impurities or when separating acetonitrile.

7. The Gas Analysis and Handling System

The intermolecular carbon-13 isotope effect was determined as a function of temperature and pressure by comparing

Figure 5.

Schematic of Bridge Circuit for Gas Chromatograph

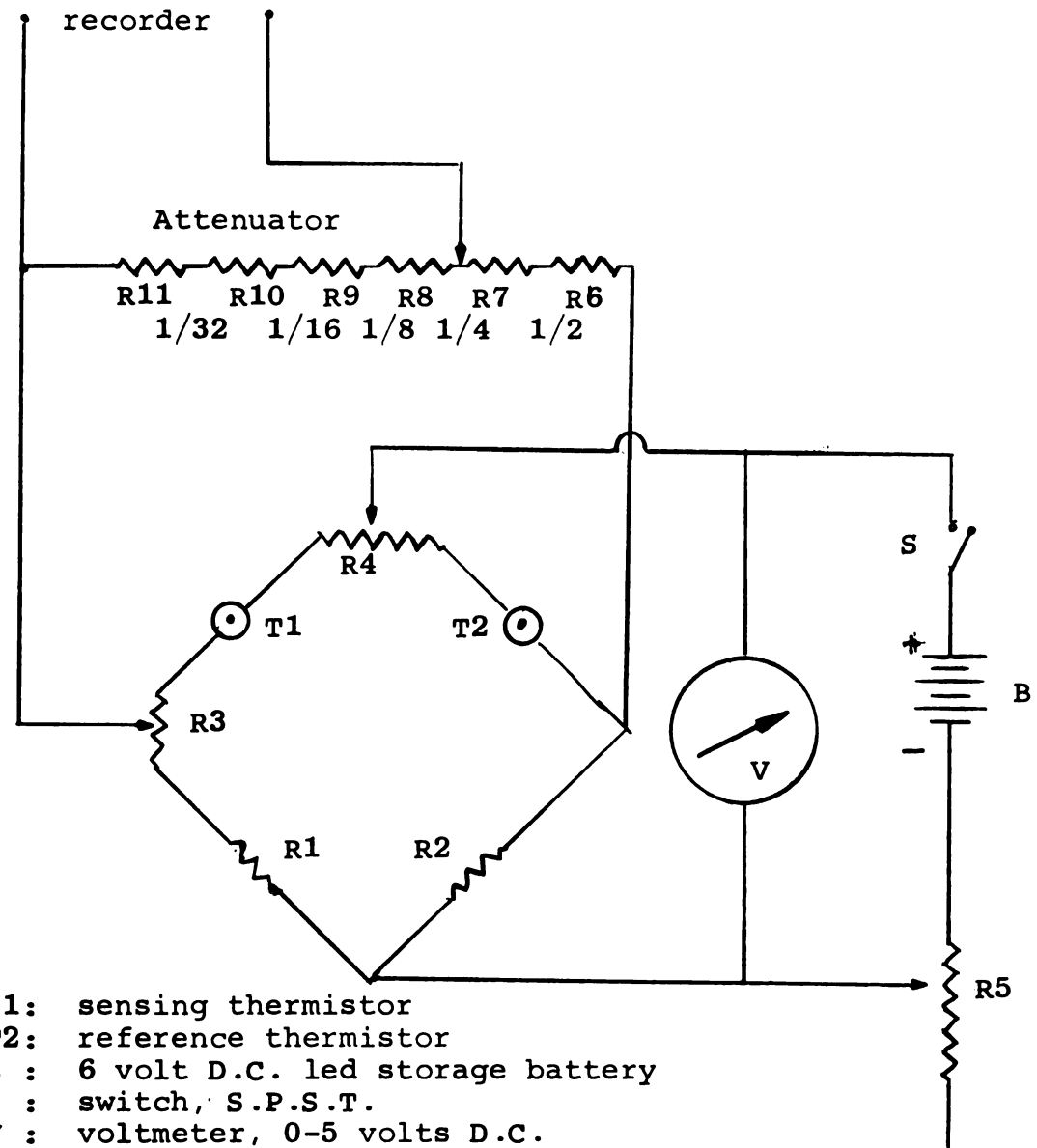

T1: sensing thermistor
T2: reference thermistor
B : 6 volt D.C. led storage battery
S : switch, S.P.S.T.
V : voltmeter, 0-5 volts D.C.
R1: 270 ohms ± 1%
R2: 270 ohms ± 1%
R3: fine zero control; 10 ohms, 10 turn Helipot
R4: coarse zero control; 1000 ohms, 10 turn Helipot
R5: voltage adjust; 500 ohms, 10 turn Helipot
R6: 400 ohms ± 1%
R7: 100 ohms ± 1%
R8: 100 ohms ± 1%
R9: 50 ohms ± 1%
R10: 25 ohms ± 1%
R11: 25 ohms ± 1%

Figure 5.

the isotope contents of the carbon dioxide obtained from combustion of methyl isocyanide and acetonitrile over copper oxide in a combustion furnace F (Figure 6) from each quenched kinetics run. The manifold, pump, and vacuum system is similar to the furnace inlet system described earlier.

C. PROCEDURE

1. Kinetics

The reactant gas, methyl isocyanide, was stored as a liquid kept constantly at dry ice temperatures in a 2 liter storage vessel ST1 (Figure 2 ,p. 31). The main sample was allowed to warm up slowly, the necessary vapor for the kinetic run distilled off, and the main sample was then re-frozen immediately. Since the vapor pressure of methyl isocyanide at room temperature is approximately 130 mm, it was necessary to use a unreactive (inert) gas, ethane, to obtain reactant pressures greater than 130 mm. The experimental procedure for the introduction of the sample into the furnace may therefore be divided into two categories: the reactions at pressures below 130 mm, in which pure methyl isocyanide vapor was used, and that forreactions at higher pressures, requiring addition of inert gas.

a. Reactant only Methyl Isocyanide

The main sample of methyl isocyanide in ST1 was allowed to warm up and expand through stopcock S6, (Figure 2, p.31) and into the inlet area through PS10, PS11, PS12,

Figure 6.

Schematic of the Gas Analysis and Handling System

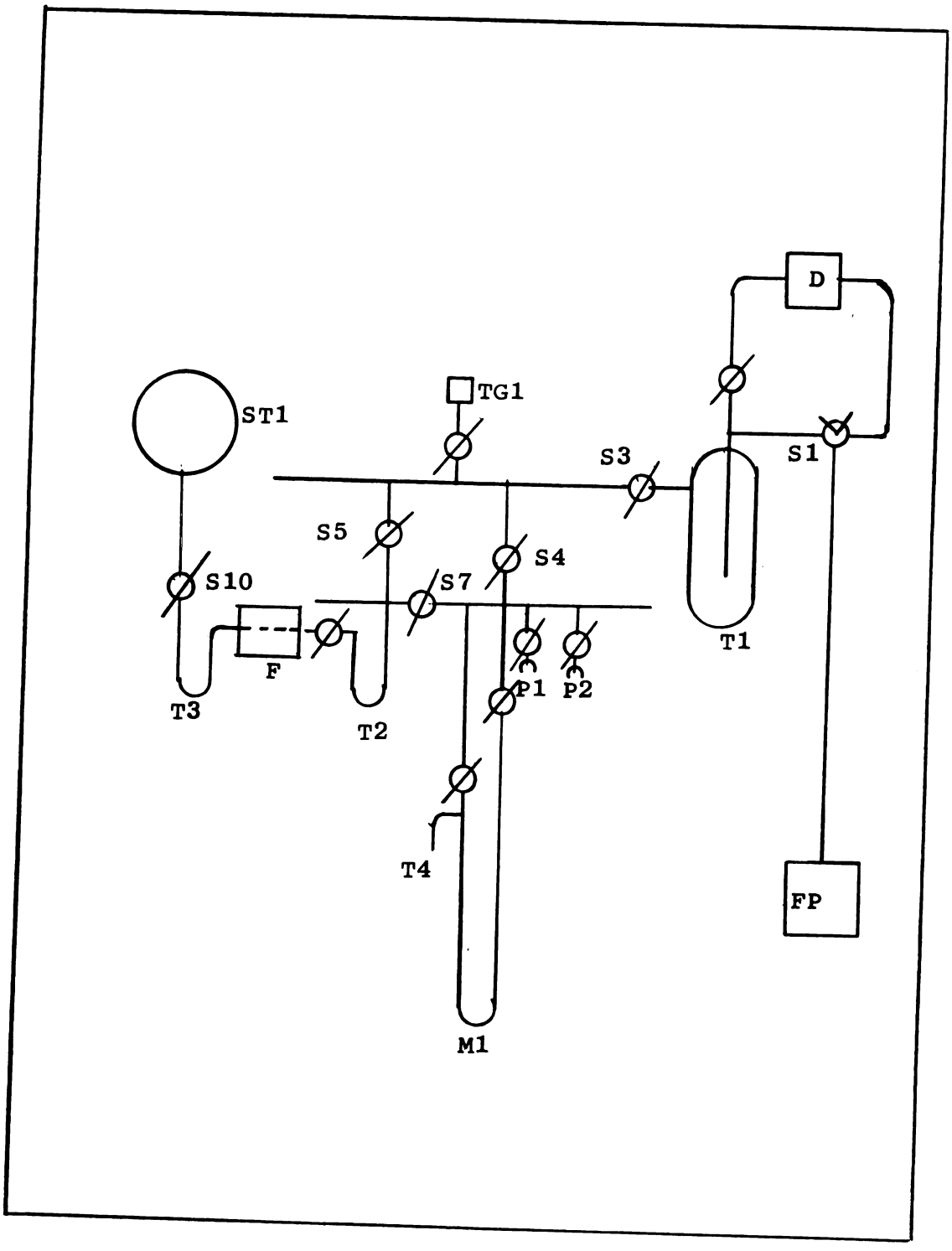

Figure 6.

and PS13. When approximately the desired pressure was recorded on manometer M1, stopcock S6 was closed. PS14 was then opened and the reactant gas allowed to expand into the preheated reaction vessel. After equilibration for 10 seconds, PS14 was closed and the time recorded. The pressure was then read from a millimeter scale attached to manometer M1. The methyl isocyanide remaining in the volume between PS14 and S6 was then frozen back into ST1.

b. Inert Gas Runs

Methyl isocyanide from ST1 was allowed to warm up and expand into a bulb B of known volume (502.9 cc) attached to port P1. When the desired pressure was recorded on M1, S8 was closed and the methyl isocyanide remaining in the vacuum system was frozen back in ST1. The contents of the bulb B were then vacuum transferred to U-Trap between PS13 and PS14.

Ethane gas was then allowed to expand from storage bulb EV1 through S5 and PS10 into the expansion volume EV2 (6000 cc). As soon as the desired pressure was recorded on M1, PS10 was closed.

The methyl isocyanide in the U-Trap was vaporized using a Dewar of boiling water and PS14 was opened, followed rapidly by opening of PS13. The methyl isocyanide was forced into the reaction vessel by the rapid expansion of ethane at higher pressure, assuring good mixing with minimum back diffusion. After equilibration for 10 seconds PS14 was closed,

and the pressure on M1 recorded. All unused ethane remaining in the vacuum system was frozen back into EV1. The effective pressure of methyl isocyanide in the reaction vessel for inert gas run was calculated from the ratio of methyl isocyanide to ethane, and the known collisional deactivation efficiency of ethane[21].

The temperature of the reaction vessel was determined from the voltage output of the several thermocouples, using a 0^0C reference point, as measured with a Leeds and Northrup Type K3 potentiometer and a Leeds and Northrup (Model 2430-A) galvanometer as a null indicator. Two volts tapped from a six-volt lead storage battery served as a working cell, with an Eppley standard cell (certified by the National Bureau of Standards as 1.01926 volts at 23^0C) as the reference cell.

Five Chromel-Alumel thermocouples and a Platinum-Platinum, 10% rhodium thermocouple, located at various points on the outer surface of the cylindrical reaction vessel, were used to determine the temperature. The voltage output of each thermocouple was converted to temperature by use of the National Bureau of Standards Reference Tables for Thermocouples (Circular 561, 1955), and the average temperature determined from all thermocouples was taken as the temperature of that particular run. (Prior calibration of the thermocouples showed that deviations from the reference table values were in all cases within experimental error).

After a time sufficient to assure the desired fraction f of reaction, the reaction was quenched by opening stopcock PS14 to trap T2, cooled with liquid nitrogen, and the time recorded. The products were removed through port P1 to a storage bulb. In the case of inert gas runs, a dry ice-alcohol bath was placed on trap T2, liquid nitrogen on the trap connected to EV1, stopcock PS14, PS13, PS10, and S5 opened, and the reaction mixture frozen out of the reactor. Methyl isocyanide and acetonitrile were retained in trap T2.

2. Separation of the Reaction Products

The storage bulb containing the reaction products (acetonitrile and unreacted methyl isocyanide) was then connected to port P1 of the gas chromatographic system (Figure 6, p. 43). Generally five introductions of 10 cm pressure in the sampling volume T2 were chromatographed through the carbowax 2 M column, which effected separation with no detectable retention of either product. The methyl isocyanide "peak" from each introduction was frozen out in trap T3 and the acetonitrile in trap T4 of the chromatographic collection system, and the separated product each removed to a storage bulb (through port P2) and reserved for combustion.

3. Combustion

A sample of methyl isocyanide (or acetonitrile) was introduced into the gas analysis section of the vacuum line

(through port P1, Figure 6, p. 43), and the amount N_i measured in the calibrated manometer M1. The gas was then vacuum transferred to furnace F. (Sargent Co., Model S-36400), containing a Vycor combustion tube filled with copper oxide wire at 600°C. After at least ten slow passes between traps T2 and T3, the products (carbon dioxide and water) were transferred to T2, cooled with liquid nitrogen. The carbon dioxide was distilled from dry ice-alcohol into trap T4, and the quantity N_f of gas measured in manometer M1. In all cases, it was required that $N_f/2N_i = 0.95$ was accomplished, or the gas was returned to the furnace for further oxidation (control experiments indicated that this level of oxidation was sufficient to assure that the measure $^{13}CO_2/^{12}CO_2$ molar ratio was representative of the ratio $(^{13}CH_3NC + CH_3N^{13}C/CH_3NC)$.

B. EQUILIBRATION

The combustion process was found to introduce non-reproducible amounts of ^{17}O and ^{18}O into the carbon dioxide rendering the 45/44 mass ratio unreliable as a measure of the $^{13}CO_2/^{12}CO_2$ ratio at the high level of precision required by the small isotope effect in the isomerization. Therefore each sample was distilled through a port P1-P4 into an equilibration bulb (a tube of about 100 cc volume attached to a stopcock) and equilbrated for at least 24 hours with 5 cc of standard conductivity water from which air and carbon dioxide contaminents had been removed. The

experimentally derived carbon dioxide was then removed and transferred to a mass spectral sample bulb for later isotopic analysis.

1. Isotopic Analysis

The $^{13}CO_2/^{12}CO_2$ molar ratio (45/44 peak ratio) of each sample of equilibrated carbon dioxide was determined with a Consolidated-Nier Model 21-201 isotope-ratio mass spectrometer at the University of Illinois

The measured 45/44 peak ratio was found to be somewhat dependent on the sample pressure introduced into the intrument. To obtain consistency, all samples were run with a sample pressure sufficient to produce an output signal of ($^{12}CO_2$) 29.5 ± 0.2 volt on the $\frac{m}{e}=44$ collector. The corrections applied to the observed "raw" 45/44 ratio, and calculations of the isotopic ratio constants ratios are discussed in the next chapter.

IV. RESULTS

A. KINETICS

The apparatus was proved by determining the apparent first-order rate constant k for each of the three temperatures 243.4, 226.0 and 213.0°C, at a number of pressures and comparing with the results of Schneider[36].

The apparent first-order rate constant is defined by

$$k = \frac{-\ln(1 - f)}{t}$$

where f is the fraction of reaction obtaining at a reaction time t. The fraction of reaction f is given in terms of the ratio A/B of methyl isocyanide/ acetonitrile in the product mixture by

$$f = [A/B + 1]^{-1} \qquad (19)$$

The ratio A/B was determined from the ratio of peak areas A_{NC}/A_{CN} on the chromatogram corresponding to methyl isocyanide and acetonitrile, respectively. The carbowax 20M column was found to have a somewhat greater sensitivity for methyl isocyanide than for acetonitrile, so that the area ratio A_{NC}/A_{CN} was calibrated with samples of known composition. The calibration was checked periodically, but no change was noted with time.

The only correction applied to the raw kinetic data was for temperature differences as large as 2°C which were

obtained between runs of a given "fall-off" group which were sometimes run several days apart. The maximum temperature fluctuation or drift occurring during the longest runs was $\pm$ 0.1°C. This correction can be derived from the Arrhenius equation 1 to be

$$\frac{\Delta k}{k} = \frac{E}{RT^2} \Delta T \quad , \qquad (20)$$

where E, the experimental activation energy, is 38.35 Kcal/mole. For instance, in one run the temperature was 244.0°C and the rate constant $k = 52.9 \times 10^{-5}$ sec^{-1}. The temperature of the "fall-off" group was 243.4°C. The correction of the rate constant for the run at 244.0°C to 243.4°C is then found to be:

$$10^2 \frac{\Delta k}{k} = \frac{38,350 \times 100}{1.98717 \times (243.4 + 273.2)^2} (0.6) = 4.34\%$$

$$k(243.4) = 50.6 \times 10^{-5} \text{ sec}^{-1}$$

This correction can also be stated in terms of a correction of the observed fraction of reaction f (244.0) = 0.603 to f (243.4°C) = 0.588.

The results are shown in Table 1 , and presented graphically in Figure 7 . Included for comparison in Figure 7 are the results of Schneider[36] at 230.4°C. The results are in excellent agreement with those of Schneider.

B. KINETIC ISOTOPE EFFECTS

For the competitive reaction of two isotopic molecules

$$A \xrightarrow{k} B$$
$$A' \xrightarrow{k'} B' \quad ,$$

Table 1 . Summary of kinetic data

Pressure (mm)	Reaction Time, t (sec)	Fraction of Reaction, f	k_{-1} (sec^{-1})
T = 243.4°C			
525	281	0.461	220×10^{-5}
438	214	0.294	214×10^{-5}
343	330	0.474	195×10^{-5}
271	330	0.455	184×10^{-5}
246	360	0.468	175×10^{-5}
159	280	0.462	146×10^{-5}
96.0	419	0.444	140×10^{-5}
62.5	544	0.450	110×10^{-5}
33.5	1200	0.590	74.3×10^{-5}
24.0	1022	0.527	73.2×10^{-5}
13.7	2100	0.619	45.9×10^{-5}
12.5	1747	0.588	50.8×10^{-5}
T = 226.0°C			
880	1076	0.483	67.6×10^{-5}
601	810	0.406	60.6×10^{-5}
475	960	0.443	60.9×10^{-5}
369	1106	0.397	45.7×10^{-5}
284	1110	0.427	50.3×10^{-5}
242	1020	0.332	39.6×10^{-5}
188	1177	0.373	39.7×10^{-5}
74.0	2340	0.511	30.5×10^{-5}
57.0	2990	0.550	26.7×10^{-5}
46.0	2567	0.479	25.4×10^{-5}
38.0	2400	0.474	26.8×10^{-5}
32.0	2400	0.411	22.1×10^{-5}
25.5	3014	0.497	22.8×10^{-5}
17.0	4451	0.602	17.4×10^{-5}
11.5	5110	0.533	14.7×10^{-5}
T = 213.0°C			
827	3656	0.518	19.9×10^{-5}
680	3719	0.505	18.9×10^{-5}
503	4272	0.605	21.7×10^{-5}
475	4911	0.597	18.5×10^{-5}
406	4383	0.558	18.6×10^{-5}
202	5161	0.550	15.5×10^{-5}
88.0	7750	0.594	11.6×10^{-5}
68.5	8086	0.610	11.6×10^{-5}
46.0	7005	0.515	10.3×10^{-5}
16.0	18000	0.680	6.33×10^{-5}

Figure 7. Experimental Rate Constants *versus* Pressure at 243.4°C, 226.0°C, 213.0°C.

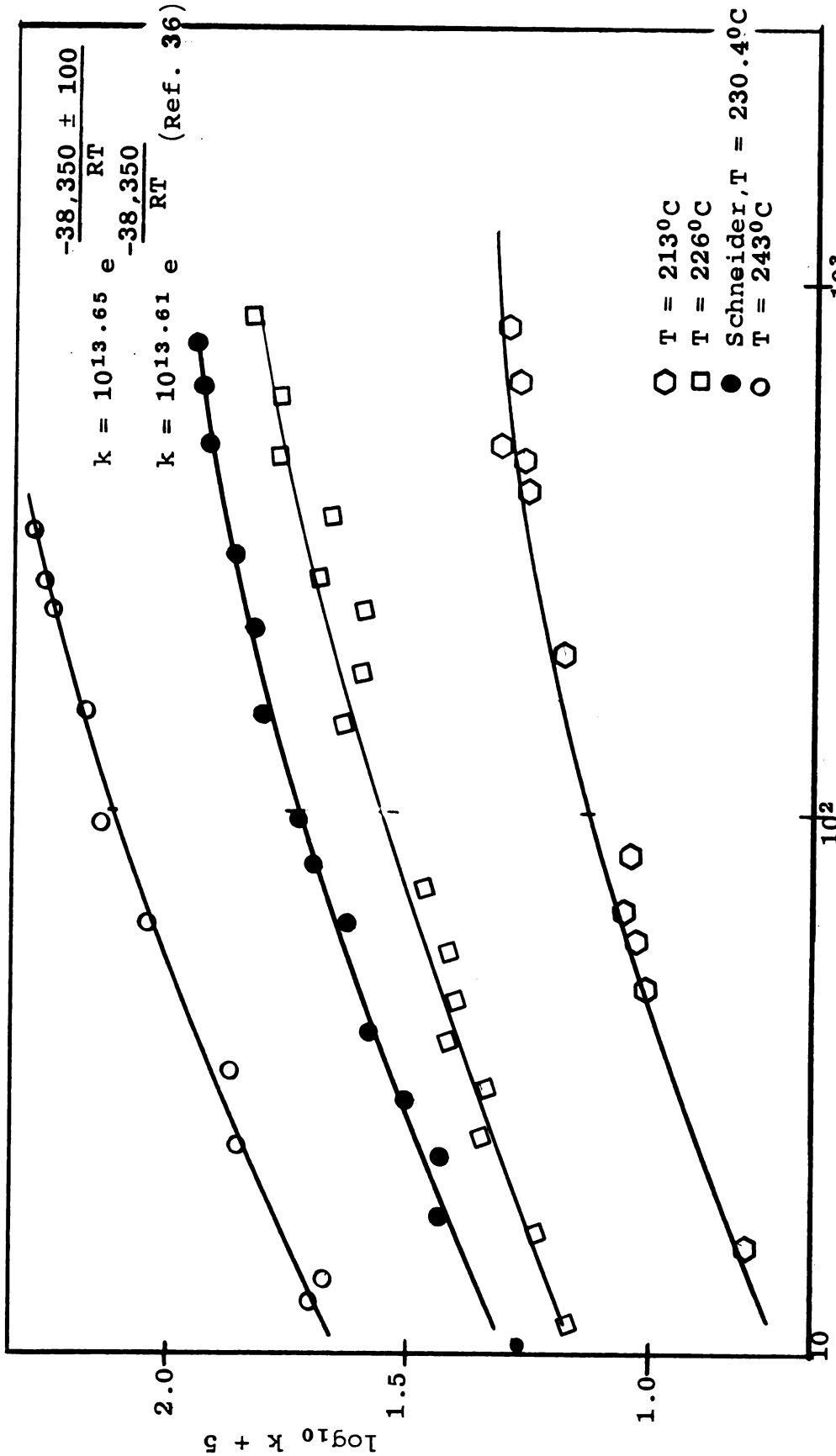
$k = 10^{13.65} e^{\frac{-38,350 \pm 100}{RT}}$
$k = 10^{13.61} e^{\frac{-38,350}{RT}}$ (Ref. 36)
T = 213°C
T = 226°C
Schneider, T = 230.4°C
T = 243°C
$\log_{10} k + 5$
2.0
1.5
1.0
10
10^2
10^3
Pressure (mm)

Figure 7.

where the prime refers to the heavier isotopic molecule, the kinetic isotope effect ϵ is defined as the deviation from unity of the isotopic rate constant ratio k/k':

$$\epsilon = \left| \frac{k}{k'} - 1 \right| \tag{21}$$

It has become somewhat conventional to refer to the isotopic rate constant ratio $r = k/k'$ itself as the kinetic isotope effect, and this convention will be adopted in the remaining discussion.

The experimental ratio r of isotopic rate constants can be determined from any three of the four data (where A, B refer to moles of A and B respectively):

$$\begin{aligned} f &= \frac{B + B'}{A_0 + A_0'} = \text{the fraction of reaction} \\ R_{A_0} \left(\equiv R_{B_\infty}\right) &= \text{the initial molar ratio } (A'/A)_0 \\ R_{A_t} &= \text{the molar ratio } (A'/A)_t \text{ obtaining at } f \\ R_{B_t} &= \text{the molar ratio } (B'/B)_t \text{ obtaining at } f. \end{aligned} \tag{22}$$

Exact expressions for r in terms of any three of the four data have been given by Yankwich and Tong [40]. The expression involving R_{A_t}, R_{B_t}, and f

$$r = \frac{\ln \left[\frac{1}{1-f} - \frac{f}{1-f} \frac{R_{B_t} - R_{A_t}}{R_{B_t} + 1} \right]}{\ln \left[\frac{1}{1-f} + \frac{f}{1-f} \frac{R_{B_t} - R_{A_t}}{R_{B_t} + 1} \right]} \tag{23}$$

has the advantage that the relative error in r is extremely insensitive to the error in f, the least precisely known (± 1%; the corresponding error generated in r is less than 0.1 %) datum. The molar ratios can be determined to at least ± 0.001% by isotope-ratio mass spectrometry.

An expression appropriate for tracer levels of A' and B', for which f may be approximated by

$$f \simeq \frac{B}{A_0}$$

is

$$r = \frac{-\ln(1 - f)}{\ln\left[\frac{R_{B_t}}{R_{A_t}}\left(\frac{f}{1 - f}\right) + 1\right]} \qquad (24)$$

This equation will be derived in the following chapter. The results from equation 24 are in excellent agreement with those calculated from equation 23 for the case of natural abundance ^{13}C. Equation 24 greatly simplifies the analysis of the results in this study.

Methyl isocyanide contains two non-equivalent carbon atoms, either of which may be labeled, so that three isotopic reactions

$$CH_3NC \xrightarrow{k} CH_3CN$$

$$^{13}CH_3NC \xrightarrow{k_1} {}^{13}CH_3CN$$

$$CH_3N^{13}C \xrightarrow{k_2} CH_3{}^{13}CN$$

need to be considered (the probability of double labeling, $^{13}CH_3N^{13}C$, is negligible at the tracer level), and two

kinetic isotope effects arise: k/k_1 and k/k_2. The experimental procedure used in this study involved determining (see Chapter III) the $^{13}CO_2/^{12}CO_2$ ratio R for carbon dioxide derived from oxidation of unreacted methyl isocyanide (R_A) and acetonitrile (R_B) accumulated to time t.

The $^{13}CO_2/^{12}CO_2$ molar ratio was taken as the 45/44 mass spectral peak ratio, corrected as follows:

(1) Contribution of the species $^{12}C^{16}O^{17}O$ to the 45 peak was made by subtracting 0.0008 from each ratio.[a]

(2) The inability of the instrument to resolve completely the large 44 peak and the 45 peak was made by subtracting 0.0002 from each ratio.[a]

(3) Instrumental response fluctuations were negated by subtracting from or adding to each sample ratio the difference between the 45/44 ratio of a standard sample of CO_2 and its accepted value. The standard was run at least once each four-hour period.

As an example of how a corrected ratio was determined, consider the following at 243.4°C and 343 mm pressure for the carbon dioxide from the combustion of methyl isocyanide.

m/e(45/44) = 0.0121341

tank CO_2: m/e(45/44) = 0.0127142

Accepted tank value= 0.0127000

0.0000142

[a]Corrections previously established in the Mass Spectrometry Laboratory of the University of Illinois.

0.0121341		
-0.0000142		tank correction
0.0121199		
-0.0008		$^{12}C^{16}O^{17}O$ correction
0.0113199		
-0.0002		resolution correction
0.0111199	⟵	corrected ratio

These ratios are related to the molar ratios of isotopic methyl isocyanide and/or acetonitrile by the conbustion reactions:

$$CH_3NC \longrightarrow 2CO_2$$

$$^{13}CH_3NC \longrightarrow {}^{13}CO_2 + CO_2$$

$$CH_3N^{13}C \longrightarrow {}^{13}CO_2 + CO_2$$

whence, the molar ratio

$$R_A = \frac{^{13}CO_2}{CO_2} = \frac{^{13}CH_3NC + CH_3N^{13}C}{^{13}CH_3NC + CH_3N^{13}C + 2CH_3NC} \qquad (25)$$

or

$$\frac{1}{RA} = 1 + 2\,\frac{CH_3NC}{^{13}CH_3NC + CH_3N^{13}C}$$

$$\frac{1}{RA} = 1 + \frac{2}{R_{NC}} \qquad (26)$$

A corresponding equation relates R_B and R_{CN}. The molar ratios $^{13}CH_3NC$ and $CH_3N^{13}C$ needed to determine separately k/k_1 and k/k_2 from either equation 23 or equation 24 cannot be obtained separately from natural abundance studies. However, the ratio R_{NC} or R_{CN} can be used in either equation 23 or equation 24 to calculate

an "average" isotope effect k/k'. If equation 24 is used a relation between the average isotope effect k/k' and the individual isotope effects k/k_1 and k/k_2 can be derived (Chapter V). Information concerning the individual isotope effects k/k_1 and k/k_2, arising from labeling the methyl and isonitrile carbons, respectively, may thus be obtained from the experimental average isotope effect k/k'. Alternatively, studies involving methyl isocyanide enriched in either the methyl or isonitrile position can be used together with the natural abundance results to obtain directly k/k_1 and k/k_2. Attempts were made to label the methyl position and obtain the separate effects k/k_1 and k/k_2 directly, but difficulties were encountered. These attempts are described in the Appendix.

The isotope effect results are given in Table 2 , , and in Figure 8 . Most effort was directed toward the experiments performed at 226°C; the results for this temperature represent the average of a large number of separate experiments at each pressure. The results at the other temperatures (243.4 and 213°C) represent single experiments at each pressure, or in some cases duplicates. The results at these temperatures are not of the same quality as those at 226°C, and were carried out mainly to determine the difference in critical energies for the isotopic molecules. It is often found that, at high pressures, the temperature dependence of the isotope effect is of the Arrhenius form:

$$(k/k')_{\infty} = Ar \exp(\Delta E_0/RT)$$

where $\Delta E_0 = E_0' - E_0$, and the critical energy E_0 is related to the observed activation energy by

$$E_0 = E_a^{\infty} + \langle E_v^* \rangle - \langle E_v^+ \rangle - RT$$

where $\langle E_v \rangle$ represents the average vibrational energy , and * and + refer to active molecule and activated complex, respectively.

The temperature dependence of the average ^{13}C isotope effect k/k' for methyl isocyanide isomerization was found to be

$$(k/k')_{\infty} = 0.998 \exp(20 \pm 5/RT) .$$

Since the temperature dependence is small, and subject to considerable experimental error, the detailed pressure "fall-off" of the isotope effect at a given temperature is more important for comparisons with theory than results of lesser quality at several temperatures.

Table 2. Summary of isotope effect data.

Pressure (mm)	f[a]	R_A[b]	R_B[c]	k/k' Calc by Eq. 24	k/k' Calc by Eq. 23
T = 243.4°C					
525	0.461	0.0110900	0.0108450	1.0170_3	1.0170_2
438	0.294	0.0110749	0.0108861	1.0148_2	1.0148_1
343	0.474	0.0111199	0.0108778	1.0165_9	1.0165_9
271	0.696	0.0111835	0.0109260	1.0139_1	1.0139_1
242	0.468	0.0111004	0.0108912	1.0143_9	1.0143_9
33	0.590	0.0110877	0.1093360	1.0094_3	1.0094_3
12.5	0.588	0.0111168	0.0109918	1.0076_2	1.0076_2
T = 226.0°C					
880	0.483	0.0111016	0.0108289	1.0186_3	1.0186_3
475	0.443	0.0111055	0.0108740	1.0162_9	1.0162_9
369	0.397	0.0111009	0.0108680	1.0170_0	1.0170_0
74.0	0.511	0.0111032	0.0108797	1.0148_3	1.0148_2
46.0	0.479	0.0111251	0.0108985	1.0154_4	1.0154_5
32.0	0.411	0.0110972	0.0109026	1.0140_1	1.0140_0
17.0	0.602	0.0111175	0.0109167	1.0121_4	1.0121_4
11.5	0.533	0.0110897	0.0108997	1.0123_3	1.0123_3
T = 213.0°C					
88.0	0.594	0.0111473	0.0108850	1.01604	1.01604
46.0	0.515	0.0111784	0.0109171	1.0172_1	1.0172_3
16.0	0.680	0.0111900	0.0109275	1.0144_8	1.0144_8

[a] Fraction of reaction.

[b] $^{13}CO_2/^{12}CO_2$ from combustion of unreacted methyl isocyanide.

[c] $^{13}CO_2/^{12}CO_2$ from combustion of the product, acetonitrile.

Figure 8. Experimental Rate Constant Ratios k/k', versus Pressure at 243.4°C, 226.0°C.

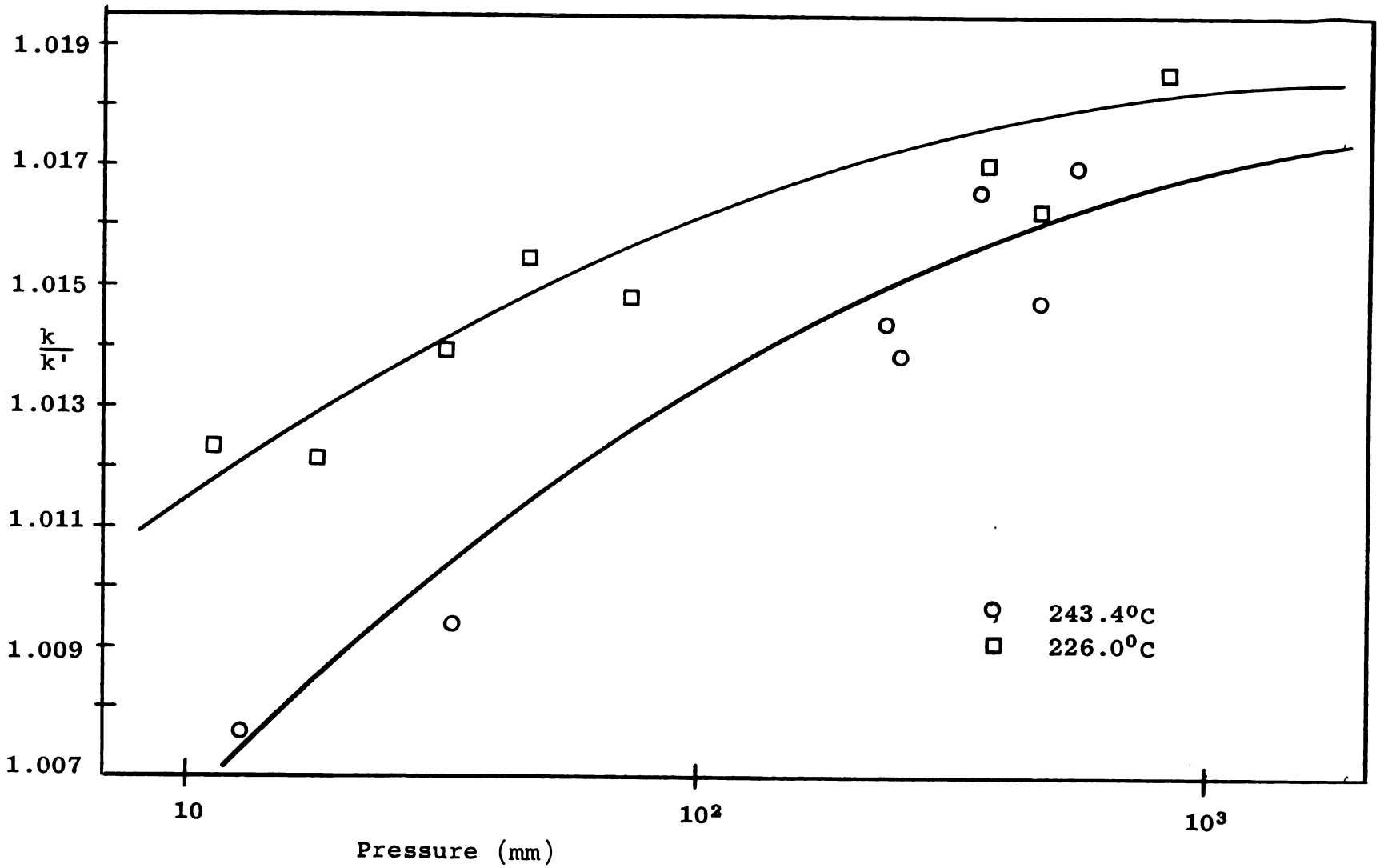
1.019
1.017
1.015
k/k'
1.013
1.011
1.009
1.007
10
10²
10³
Pressure (mm)
243.4°C
226.0°C

Figure 8.

V. DISCUSSION

A. RELATION OF THE AVERAGE ISOTOPE EFFECT TO LABELING AT THE METHYL AND ISONITRILE POSITION

The experimental method used in this study involved determination of the $^{13}CO_2/^{12}CO_2$ ratio R on samples of carbon dioxide derived from oxidation of unreacted methyl isocyanide (R_A) and acetonitrile (R_B) accumulated to time t or fraction f of reaction. As discussed in the last chapter, R_A and R_B can simply be related to the molar ratios of isotopic methyl isocyanides and acetonitriles,

$$R_{NC} = \frac{^{13}CH_3NC + CH_3N^{13}C}{CH_3NC}$$

(R_{CN}), respectively. The ratios R_{NC} and R_{CN} and f can then be used to calculate an isotope effect k/k' which is an "average" of the position isotope effects arising from labeling the methyl (k/k_1) and the isonitrile (k/k_2) carbons, by the use of the exact expression of Yankwich and Tong.[40] The exact relationship between k/k' and the individual position isotope effects k/k_1 and k/k_2 can be derived by use of an approximation which has high validity for the case of tracer (natural abundance ^{13}C) labeling, as discussed earlier. The approximate equation can be derived simply as follows: Consider the competitive first-order reactions of isotopic molecules A and A', with rate constants k and k', respectively:

$$A \xrightarrow{k} B$$

$$A' \xrightarrow{\quad k' \quad} B' \ ,$$

where the prime refers to the heavier isotopic molecule. The isotope effect will be defined as $r = k/k'$. Following Yankwich and Tong[40] the fraction of heavy isotopic molecules remaining at t can be written:

$$g = \frac{A'}{A'_0} = e^{-k't} \tag{27}$$

The corresponding fraction for the light molecules is

$$\frac{A}{A_0} = e^{-kt} = e^{-k'(\frac{k}{k'})t} = g^r \tag{28}$$

The isotopic ratios of molecules of A remaining (R_{At}) and of product B accumulated (R_{Bt}) to t are then

$$R_{At} = \left(\frac{A'}{A}\right)_t = \frac{R_0}{g^{r-1}} \tag{29}$$

$$R_{Bt} = \left(\frac{B'}{B}\right)_t = \frac{R_0(1 - g)}{1 - g^r} \tag{30}$$

where $$R_0 = \left(\frac{A'}{A}\right)_0 = \left(\frac{B'}{B}\right)_\infty \tag{31}$$

the fraction of reaction f is

$$f = \frac{B + B'}{A_0 + A'_0} = \frac{(A_0 + A'_0) - (A + A')}{A_0 + A'_0} = \frac{(1-g^r) + R_0(1-g)}{1 + R_0} \tag{32}$$

Elimination of g from equations 29, 30, and 31 leads to the exact expression for r:

$$r = \frac{k}{k'} = \frac{\ln\left[\left(\frac{1}{1-f}\right) + \left(\frac{f}{1-f}\right)\cdot\frac{R_{At} - R_{Bt}}{(R_{Bt}+1)}\right]}{\ln\left[\left(\frac{1}{1-f}\right) - \left(\frac{f}{1-f}\right)\cdot\frac{R_{At} - R_{Bt}}{R_{At}(R_{Bt}+1)}\right]} \qquad (33)$$

The approximate expression is derived by realizing that for tracer level labeling $A'/A << 1$ at all times, and hence

$$f \cong \frac{B}{A_0} = \frac{A_0 - A}{A_0} = 1 - \frac{A}{A_0} = 1 - g^r \qquad (34)$$

Elimination of g from 29 , 30 and 34 , and rearrangement yields

$$r = \frac{\ln(1-f)}{\ln\left[\frac{R_{Bt}}{R_{At}}\,\frac{f}{1-f} + 1\right]} \; . \qquad (35)$$

An error analysis of equation 35 results in the following expression for the relative error in r:

$$\left(\frac{\Delta r}{r}\right)^2 = \left[\left(\frac{f}{1-f}\right)\left(\frac{r-1}{\ln(1-f)}\right)\right]^2 \left(\frac{\Delta f}{f}\right)^2 + 2\left(\frac{r\,f}{\ln(1-f)}\right)^2 \left(\frac{\Delta R}{R}\right)^2 \qquad (36)$$

where the relative error in f, $\frac{\Delta f}{f}$, was taken to be 1%, and the relative errors in R_A and R_B, $\frac{\Delta R}{R}$, were both taken as 0.01%. A representative value of 1.02 was assumed for the isotopic rate constant ratio r. This represents the limiting maximum value observed for the C-13 isotope effect in this study.

The variation of $\frac{\Delta r}{r}$ with fraction of reaction is shown in Figure 9 . An expression similar to equation 33 but employing input data R_0, R_{Bt}, and f, has been

derived by Bigelisen and Allen[41] , using the same approximation to f as described here. The error analysis on their equation shows that the relative error in r is much larger at all fractions of reaction for the same parameters assumed above. Exact expressions requiring as input data R_0, R_{Bt}, f; R_0, R_{At}, f; R_0, R_{At}, R_{Bt} and the relative errors obtaining in r have been discussed by Yankvich and Tong[40] , and show that the equation requiring R_{At}, R_{Bt}, f, are much less sensitive to errors in f than the other three cases. Values of R_{NC} and R_{CN} were used in place of R_{Bt} and R_{At} in equation 35; resulting values of r have been presented in Table 2. Comparison of the values shows that equation 35 is an excellent approximation to the exact expression 33 for natural abundance ^{13}C levels.

The reactions of the isotopic methyl isocyanides can be written

$$A \xrightarrow{k} B$$

$$A_1 \xrightarrow{k_1} B_1$$

$$A_2 \xrightarrow{k_2} B_2$$

where

$$A \equiv CH_3NC ,$$

$$A_1 \equiv {}^{13}CH_3NC$$

$$A_2 \equiv CH_3N{}^{13}C$$

and B, B_1, B_2 refer to the corresponding isotopic acetonitriles.

Figure 9. Relative Error in the Approximate Isotope Ratio Calculations *versus* Fraction of Reaction.

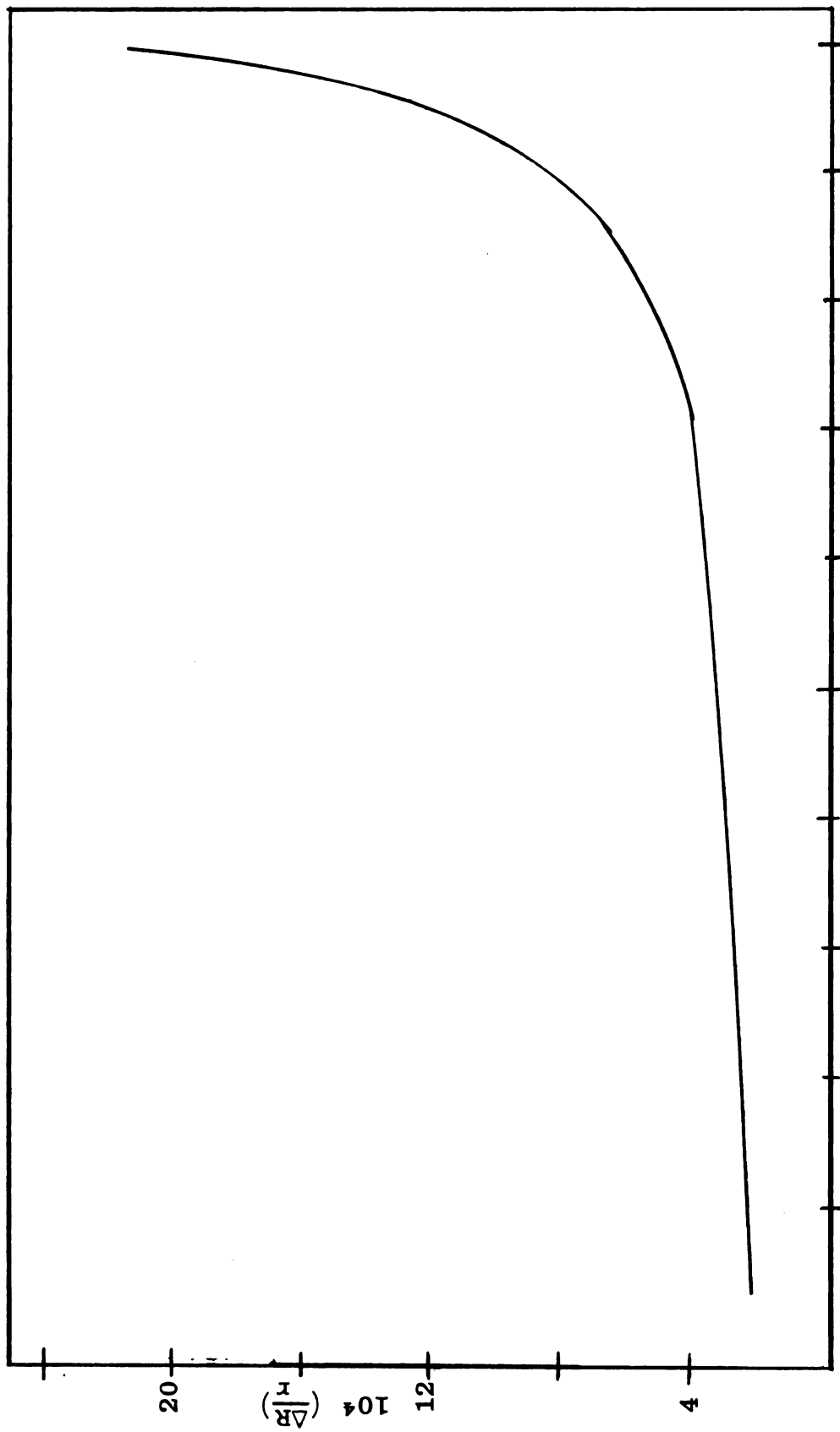
20
12
4
$10^4 \left(\frac{\Delta R}{r}\right)$
0.1
0.3
0.5
0.7
0.9
1.0
Fraction of Reaction f

Figure 9.

Let $$R_A = A_1/A \quad , \quad R_{B_1} = B_1/B$$
$$R_{A_2} = A_2/A \quad , \quad R_{B_2} = B_2/B \qquad (37)$$

and $$R_0 = (A_1/A)_0 = (A_2/A)_0 ,$$

assuming both the methyl and isonitrile carbons are labeled to natural abundance in the starting material (confirmation of this assumption comes from the fact that the $^{13}CO_2/^{12}CO_2$ ratio for samples of completely oxidized methyl isocyanide were observed to be twice the natural ^{13}C abundance).

The ratio R_{NC}/R_{CN} defined for the average isotope effect is then simply related to R_{A_1}, R_{A_2}, R_{B_1}, R_{B_2} by

$$\frac{R_{NC}}{R_{CN}} = \frac{R_{A_1} + R_{A_2}}{R_{B_1} + R_{B_2}}$$

which can be rearranged to

$$\left(\frac{R_{CN}}{R_{NC}}\right)^{-1} = \left[\frac{R_{B_2}}{R_{A_2}} + \frac{R_{B_1}}{R_{A_2}} \cdot \frac{R_{A_1}}{R_{A_2}}\right]^{-1} + \left[\frac{R_{B_1}}{R_{A_1}} + \frac{R_{B_2}}{R_{A_2}} \cdot \frac{R_{A_2}}{R_{A_1}}\right]^{-1} \qquad (38)$$

The ratios $\frac{R_{B_1}}{R_{A_1}}$, $\frac{R_{B_2}}{R_{A_2}}$, $\frac{R_{A_2}}{R_{A_1}}$, can be derived as follows:

Define fractions of A_1 and A_2 remaining at time t by:

$$g_1 = \frac{A_1}{A_{10}} = e^{-k_1 t}$$
$$g_2 = \frac{A_2}{A_{20}} = e^{-k_2 t} \qquad (39)$$

and the isotope effects

$$r_1 = k/k_1$$

$$r_2 = k/k_2 \quad .$$

The fraction of A remaining at t is then

$$A/A_0 = g_1^{r_1} = g_2^{r_2} = 1 - f \quad , \tag{40}$$

employing the same approximation for f as in the derivation of equation 34.

Then

$$R_{A_1} = \frac{R_0}{g_1^{r_1-1}} \quad ; \quad R_{A_2} = \frac{R_0}{g_2^{r_2-1}}$$

$$R_{B_1} = \frac{R_0(1 - g_1)}{1 - g_1^{r_1}} \quad ; \quad R_{B_2} = \frac{R_0(1 - g_2)}{1 - g_2^{r_2}} \tag{41}$$

Combining equations 40 and 41:

$$\frac{R_{B_1}}{R_{A_1}} = \frac{1 - f}{f}\left[\frac{1 - (1 - f)^{1/r_1}}{(1 - f)^{1/r_1}}\right]$$

$$\frac{R_{B_2}}{R_{A_2}} = \frac{1 - f}{f}\left[\frac{1 - (1 - f)^{1/r_2}}{(1 - f)^{1/r_2}}\right] \tag{42}$$

$$\frac{R_{A_2}}{R_{A_1}} = \frac{(1 - f)^{1/r_2}}{(1 - f)^{1/r_1}} \quad .$$

Equations 41 are valid for any value of f. Since most of the experiments in this study were carried to $0.4 \leq f \leq 0.6$ (See Table 1), a value of $f = 0.5$ was used in the calculations of the average isotope effect to be described.

Theoretical values for the average isotope effect k/k' at each pressure were then calculated from values of

r_1 and r_2 calculated from RRKM theory and various complex models as follows:

The calculated values of r_1 and r_2 were used to obtain values of the ratios in equation 42 for a value of $f = 0.5$. These ratios were then substituted into equation 38 and a value of R_{CN}/R_{NC} obtained. The ratio R_{CN}/R_{NC} can then be used for calculation of a theoretical average isotope effect from equation 35 .

B. CALCULATION OF THE CARBON-13 ISOTOPE EFFECT USING THE RRKM THEORY

RRKM expression for the rate constant is

$$k_{RRKM} = \alpha \frac{kT}{h} \frac{I_r}{Q_v} e^{-E_c/RT} \int_{E^+=0}^{\infty} \frac{\sum_{E_v^+ \leq E^+} P(E_v^+) \cdot e^{-E^+/RT}}{\sum P(E_v^+)} \frac{dE^+}{RT} \Bigg/ \left(1 + \frac{\alpha I_r}{ZPh} \frac{\sum_{E_v^+ \leq E^+} P(E_v^+)}{N^*(E^*)}\right) \qquad (43)$$

where the symbols have been defined in Chapter II. The detailed steps in the evaluation of k_{RRKM} for methyl isocyanide isomerization are as follows.

1. Construction of an Activated Complex

The activated complex for the isomerization of methyl isocyanide was constructed as in transition state theory,[30] so that the complex had all the properties of a normal molecule except that one of the frequencies of the reactant molecule was assumed to become an internal translation motion corresponding to the reaction coordinate. The translation is considered to have a zero or imaginary frequency, and thus one molecule frequency is removed in forming the vibrational frequency pattern of the complex. Other molecule frequencies are changed in a logical manner and adjusted to give agreement with the entropy of activation at high pressures. In addition, the frequency pattern of isotopic complexes are adjusted so that the Teller-Redlich product rule[42] is satisfied, as it is for the reactant molecules.

The molecular structure of methyl isocyanide has been determined using a variety of techniques including infrared,[43] Raman,[43] and microwave,[44] to be a symmetric-top molecule, although bent resonance structures might contribute slightly.

The molecular parameters of Gordy and coworkers[44] are commonly accepted:

$$d(C\text{-}H) = 1.094\ \text{Å}$$
$$d(C\text{-}N) = 1.427\ \text{Å}$$
$$d(N\equiv C) = 1.167\ \text{Å}$$
$$\angle(HCH) = 109^0\ 46'$$
$$\angle(CNC) = 180^0$$

A prescription for construction of the activated complex for methyl isocyanide isomerization has been offered by Schneider and Rabinovitch.[15] The rearrangement due to isomerization is described as a type of 1-2 shift similar to the Wolff rearrangement.[45] In 1-2 shifts the intermediate is assumed to have a ring structure. For methyl isocyanide, a structure such as

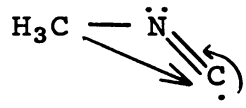

may be written. The formation of the complex can occur by way of the linear CNC bending vibration of methyl isocyanide; the bending vibrations increase the importance of bent resonance structures which contribute negligibly to the structure of the normal "linear" molecular configuration.

Three possible resonance structures may be considered:

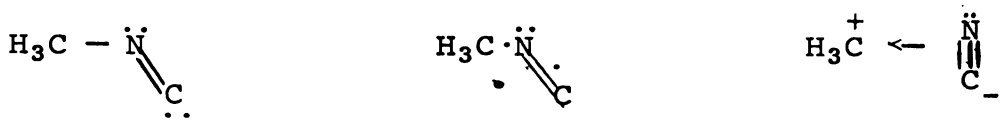

Bond orders may be defined for each structure, and the "average" distances in the activated complex 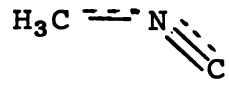 obtained by means of Pauling's bond order-bond length rules[46]

$$d(C \_\_ N) = 1.61 \text{ Å}$$
$$d(N = C) = 1.21 \text{ Å}$$
$$d(C \text{ -- } C) = 2.11 \text{ Å}$$

By trigonometry the bond angles are found to be

$$\angle (C - N - C) = 95^0\ 50'$$
$$\angle (C_M\text{-}C_N\text{-}N) = 28^0\ 57'$$
$$\angle (C - C - N) = 55^0\ 13'$$
$$\angle (H\text{-}C\text{-}H) = 109^0\ 46' \text{ (unchanged)}$$

2. Calculations of the Vibration Frequencies

The normal frequencies of vibration for all isotopic recatant molecules were calculated by Wilson FG matrix methods,[42] using a modification of a program coded by Schachtschneider.[47] A generalized valence force field was assumed.

Force constants for methyl isocyanide were taken from a vibrational analysis of CH_3NC by Pillai and Cleveland[48] A tabulation of these potential constants is given in Table 3.

Table 3. Potential constants for methyl isocyanide**

Description	Co-ordinate Pair	Force Constant***
bond stretching	N≡C	16.8500
bond stretching	C-N	5.1300
bond stretching	C-H	4.9160
bond-bond interaction	C-N; C-H	0.8000
bond-bond interaction	C-H; C-H	0.0770
angle bending	H-C-H	0.4591
angle bending	H-C-N	0.5310
angle bending	C-N-C	0.1879
angle-angle interaction	H-C-H; H-C-H	-0.0910
angle-angle interaction	H-C-H; H-C-N	-0.0767
angle-angle interaction*	H-C-H; H-C-N	-0.0599
angle-angle interaction	H-C-N; H-C-N	-0.1240

*These two angles do not have a side in common.

All other interaction constants were taken to be zero.

** M.E.K. Pillai and F. F. Cleveland, J. Mol. Spec., 5, 212 (1960).

*** Units: millidynes/Å.

The frequencies of $^{13}CH_3NC$ and $CH_3N^{13}C$ were calculated using the same potential constants. The results are presented in Table 4; included for comparison are the observed frequencies for CH_3NC.

3. The Inertial Ratio, I_r

The inertial ratio is defined as the ratio of the partition function for adiabatic rotations of the activated complex to that of the active molecule:[31]

$$I_r = \frac{Q^+_{rot}}{Q^*_{rot}} = \left(\frac{I^+_A \; I^+_B \; I^+_C}{I^*_A \; I^*_B \; I^*_C} \right)^{1/2} \qquad (44)$$

where I_A, I_B, and I_C are the principal moments of inertia. The superscripts + and * refer to the activated complex and active molecule, respectively.

4. The Reaction Path Multiplicity

The symmetry numbers usually associated with the rotational partition functions are incorporated into α, the reaction path multiplicty, which represents the number of equivalent but distinguishable reaction paths from reactants to products. Marcus[49] and Bishop and Laidler[50] have given recipes for determing α for any reaction. The transition state formulation yields

$$\alpha = \sigma/\sigma^+$$

for a unimolecular reaction, where σ is the rotational symmetry number for the active molecule and σ^+ is that

Table 4. Observed and calculated frequencies and principal moments of inertia of isotopic methyl isocyanide molecules

CH_3NC Calc.	Obs.[A]	$^{13}CH_3NC$ Calc.	$CH_3N^{13}C$ Calc.	Assignment
3017	3014	3004	3017	C-H stretch
3017	3014	3004	3017	C-H stretch
2970	2966	2966	2970	C-H stretch
2134	2166	2134	2095	N≡C stretch
1480	1467	1478	1480	CH_3 deformation
1480	1467	1478	1480	CH_3 deformation
1342	1429	1326	1341	CH_3 deformation
1011	1041	1004	1011	CH_3 rock
1011	1041	0114	1011	CH_3 rock
910	945	897	902	C-N stretch
274	263	274	272	C-N-C bend
274	263	274	272	C-N-C bend
I_A = 3.200		3.202	3.204	
I_B = 50.35		51.77	52.19	
I_C = 50.35		51.77	52.19	

Units: frequencies, cm^{-1}; moments of inertia, 10^{-40} g cm^2.

[A] M.E.K. Pillai and F. F. Cleveland, J. Mol. Spec., 5, 212 (1960).

of the complex. For methyl isocyanide (symmetry group C_{3v}) the symmetry number is 3 while that of the complex (symmetry group C_s) is 1. A difficulty arises in choosing the proper values of α for a kinetic isotope effect between two isotopic molecules, where the two have different symmetries (isotopic atoms are considered non-equivalent) and hence different reaction path multiplicities. In the case of methyl isocyanide the reaction path multiplicity is 3 for each of the isotopic molecules CH_3NC, $^{13}CH_3NC$, and $CH_3N^{13}C$, due to the presence of the 3-fold symmetry axis in each of the molecules.

5. The Vibrational Partition Function Q_v

Since only energy in excess of the zero-point energy (non-fixed vibrational energy) is available, the vibrational partition function will not contain the zero point energy and thus may be expressed[31]

$$Q_v = \prod_{i=1}^{3N-6} [1 - \exp(- h\nu_i/kT]^{-1} , \qquad (45)$$

where ν_i are the normal vibration frequencies of the molecule.

6. The Critical Energy, E_c

The critical energy is related to the experimental high-pressure activation energy, E_a, and the average vibrational energies, $\langle E_v \rangle$, of complex and active molecules by[31]

$$E_c = E_a + \langle E_v^* \rangle - \langle E_v^+ \rangle - RT \qquad (46)$$

* and + referring to the active molecule and activated complex, respectively. The average vibrational energy is given by

$$\langle E_v \rangle = \sum_i \frac{h\nu_i \exp(-h\nu_i/kT)}{1 - \exp(-h\nu_i/kT)} \qquad (47)$$

The critical energy E_c is the difference between the lowest transitional rotational vibrational state of the complex and the active molecule. For two isotopic molecules A and A' with rate constant k and k', respectively, the temperature dependence of the high-pressure isotope effect $(k/k')_\infty$ can often be expressed by an Arrhenius equation:

$$(k/k')_\infty = A_r \exp(\Delta E_a/RT) \qquad (48)$$

where $\Delta E_a = E_a' - E_a$, the difference in experimental activation energies for the isotopic molecules.

The high-pressure limit of the RRKM rate constant expression (Equation 25) leads to an expression for the high-pressure isotope effect:

$$(k/k')_\infty^{RRKM} = \left(\frac{I_r}{I_r'}\right)\left(\frac{Q_v'}{Q_v}\right)^*\left(\frac{Q_v}{Q_v'}\right)^+ \exp(\Delta E_c/RT). \qquad (49)$$

where $\Delta E_c = E_c' - E_c$, the difference in critical energies for the isotopic molecules. From the physical significance of E_c, it must be temperature-independent. However, equation 46, (which gives an approximate value of E_c by

forcing the high-pressure RRKM rate constant to have an Arrhenius temperature dependence) yields a value of E_c which is very slightly temperature dependent, since $\langle E_v \rangle$ and RT are temperature dependent. Typical values of E_c are 40-60 kcal/mole, and a change of 20-50 cal/mole for a temperature interval of 50^0C near 500^0C may result for these reactions. This is a small temperature dependence, but if both E_c and E_c' are evaluated using equation 46 an error comparable to the total magnitude of ΔE_c (20 cal/mole for C-13 isotope effects) may well result, and large errors in k/k' may be introduced. This difficulty may be avoided by realizing that

$$\Delta E_c = (E_z - E_z')^* - (E_z - E_z')^+ \qquad (50)$$

(See Figure) Therefore, the following procedure was adopted in the calculations; for the light isotopic molecule, E_c was calculated from equation 46. ΔE_c was then evaluated using equation 50 , and the critical energy for the heavy isotopic molecule calculated from

$$E_c' = E_c + \Delta E_c$$

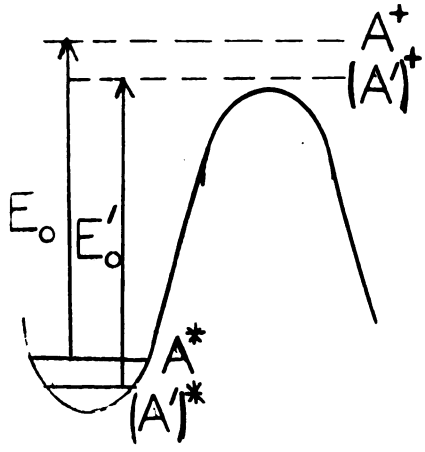

7. The Collision Frequency $\omega = ZP$

The strong collision assumption was used in all calculations. The assumption affects the positioning of the isotope effect vs. pressure curves (isotope fall-off curves) but not the fall-off shape. The net effect of the assumption is to replace the actual pressure P by an effective pressure λP, where λ is a coefficient for collisional deactivation efficienty. In comparisons with theory, the shape of the isotope fall-off curve, rather than the positioning of the curve along the pressure axis, is of importance. Very little is known of the quantitative validity of the strong collision assumption, but avlues of $0.1 \leq \lambda \leq 1$ are usually sufficient to correct the positioning of the isotope fall-off curve. Values of $\lambda = 1$ were assumed in the calculations.

The kinetic theory collision frequency was calculated from the expression 51:

$$Z = 4\left(\frac{kT}{m}\right)^{1/2} \sigma^2 \frac{N}{RT} \text{ sec}^{-1}\text{mm}^{-1} \qquad (51)$$

where N = Avogadro's number, and R = gas constant in cc mole^{-1} deg^{-1}.

8. The Calculation of $\Sigma P(E_v^+)$

The vibrational degeneracy was calculated using direct count method[38] for $E^+ \leq 0.5\ E_z^+$, the zero-point energy of

the complex, and by an approximate equation due to Whitten and Rabinovitch [52] for higher energies. The contribution to the overall rate of molecules in which $E^+ \leq 0.5\ E_z^+$ is very small, so that an almost negligible error is introduced by using an approximate expression for $\Sigma P(E_v^+)$ at these energies; however, the direct count method is onerous at these energies even for methyl isocyanide and the computer time required for evaluation of $\Sigma P(E_v^+)$ was reduced from about 5 min per run to about 1 min per run by use of the approximate expression.

9. The Density of Active Energy States $N^*(E^*)$

Since $N^*(E^*)$ is the number of vibrational quantum states of the active molecule per unit energy, it is related to the vibrational degeneracy $P(E_v^*)$ by

$$N^*(E^*) = \frac{\partial \sum_{E_v^* \leq E^*} P(E_v^*)}{\partial E^*} \qquad (52)$$

At the high energies E^* involved for the active molecule, the expression of Whitten and Rabinovitch [52] is an excellent approximation to $\Sigma P(E_v^*)$. This expression may be used to evaluate $N^*(E^*)$ as follows:

The approximate expression for $\Sigma P(E_v^*)$ is

$$\log_{10} \Sigma P(E_v^*) = s \log_{10}(E' - 1 + \beta\omega) + C \qquad (53)$$

where s = number of active vibrational degrees of freedom

$E' = E^*/E_z^*$ where E_z^* is the zero-point energy of the active molecule.

β is a frequency dispersion parameter given by

$$\beta = \frac{s - 1}{s} \frac{\langle \nu^2 \rangle}{\langle \nu \rangle^2}$$

where $\langle \nu^2 \rangle$ is the mean square frequency and $\langle \nu \rangle$ is the mean frequency of the active molecule, and ω is an empirical parameter given by the relations

$$\log_{10} \omega = -1.0506 \, (E')^{0.25} \qquad \text{for} \quad 1.0 \leq E' \leq 8.0$$

$$\omega^{-1} = 5E' + 2.73 \, (E')^{0.50} + 3.5100 \quad \text{for} \quad 0.1 \leq E' \leq 1.0$$

and the constant C is given by

$$C = s \log_{10} E_z^* - \log_{10} s! - \sum_{i=1}^{s} \log_{10} (h\nu_i)$$

To evaluate $N^*(E^*)$ we write

$$N^*(E^*) = \frac{\partial \sum P(E_v^*)}{\partial E^*} = P(E_v^*) \frac{\partial \ln \sum P(E_v^*)}{\partial E^*} \qquad (54)$$

but from equation 52

$$\frac{\partial \ln \sum P(E_v^*)}{\partial E^*} = \frac{s}{E_z^*(E' + 1 - \beta\omega)}$$

and hence

$$N^*(E^*) = \frac{s}{E_z^*(E' + 1 - \beta\omega)} \; P(E_v^*) \qquad (55)$$

10. Evaluation of the RRKM Integral

Equation 43 for k_{RRKM} contains a semi-definite integral (i.e., one of the integration limits is infinity) I_{RRKM}; however, examination shows the integrand has an appreciable

magnitude only at small values of the integration variable E^+ and decreases nearly exponentially at high energies. The contribution to the integral at high energies is very small, with the result that the integral can be approximated closely by a definite integral in which the upper integration limit is chosen to assure a small error.

Simpson's rule[53] was used for numerical integration of I_{RRKM}. It was shown to fit an analytical test expression, having the same general characteristics as the I_{RRKM} integrand, to better than 6 decimal places. In addition since it is known that the limit of high pressures of the RRKM integral is the vibrational partition of the complex Q_v^+, which can be calculated exactly from complex frequencies.

$$\lim_{P \longrightarrow \infty} I_{RRKM} = Q_v^+ \qquad (56)$$

The integration limit E_{max}^+ was chosen so that the error in the integrated partition function was less than 0.1%

C. COMPARISON OF EXPERIMENT AND RRKM THEORY

1. Activated Complex Models

The geometry and bond orders assumed for all of the complex models have been described in Section B of this chapter. Several different complex models, differing only in the vibrational frequency were constructed and the results were examined by comparison with the experimental "average" isotope effect, as described previously. For the calculation of r_1 and r_2 (isotope effects arising from labeling at the methyl and isonitrile position, respectively), vibrational frequency patterns for the complexes (CH_3NC^+), $(^{13}CH_3NC)^+$, and $(CH_3N^{13}C)^+$ are required The prescription for constructing the two "types" of complexes (i.e., two different complex vibrational frequency patterns, referred to as the 8/30 and 10/40 complexes) giving the best overall agreement with experiment was as follows. One of the degenerate CNC bending modes of methyl isocyanide was considered to become internal translational motion along the reaction coordinate in going to the complex, and the frequency was removed from the set of complex frequencies, as required in transition state and RRKM theories. The C-N and N≡C stretching frequencies of methyl isocyanide were lowered 30 or 40% and 8-10% corresponding to the 8/30 or 10/40 complex model, respectively. In addition the degenerate (species E) C-H stretching frequencies of methyl isocyanide were lowered 0.2% (the frequencies for

methyl isocyanide are 3014 (2) cm^{-1}, and for acetonitrile 3009 cm^{-1})[48]. For the 8/30 model, the remaining CNC bending frequency was raised 10% (respective molecule frequencies are: CNC bend, 270 cm^{-1}, methyl isocyanide; 361 cm^{-1} acetonitrile). All other molecule frequencies were assumed not to change in going to the complex. These changes are summarized in Table 5. The complex frequencies determined by these rules for the isotopic molecules A_1 and H_2 ($^{13}CH_3NC$ and $CH_3N^{13}C$, respectively) were adjusted slightly in the final frequency pattern in order to (1) satisfy the Teller-Redlich product rule , and to insure the correct ΔE_c between the isotopic molecule A_1 or A_2 and unlabeled methyl isocyanide, A. The observed experimental activation energy difference for the average isotope effect r was ΔE_a = 20 ± 5 cal/mole. The temperature dependences (expressed as ΔE_c) of the isotope effects r_1 and r_2 are not known precisely, but from comparison with the results from other systems , would not be expected to be very different from one another nor from the value 20 cal/mole; consequently, ΔE_c for both r_1 and r_2 was assumed to be 20 cal/mole, and the vibrational frequency pattern of the isotopic molecules A_1 or A_2 were adjusted as described in Section B in order to insure this value. This did not require adjustment by more than 2 or 3 cm^{-1} in any frequency from the values determined using the prescription of Table 5. In the case of $^{13}CH_3NC$ this value of ΔE_c could not be obtained by small adjustments unless the C-H and

Table 5. Construction of the complex models.

Molecule Frequency	Complex Frequency 8/30	10/40
Species A_1		
C-H stretch	unchanged	unchanged
N≡C stretch	lowered 8%	lowered 10%
CH_3 deformation	unchanged	unchanged
C-N stretch	lowered 30%	lowered 40%
Species E		
C-H stretch	lowered 0.2%	lowered 0.2%
CH_3 deformation	unchanged	unchanged
CH_3 rock	unchanged	unchanged
CNC linear bending	one deleted, one raised 10%	one deleted, one unchanged

CNC frequencies were assumed to change as shown in Table 5. The prescription in Table 5 corresponds rather closely, to that given by Schneider and Rabinovitch[15] (for the 10/40 model) and more recently by Rabinovitch, et al.[21] for the 8/30 model, except that the C-H and remaining CNC bending frequencies were assumed not to change by these workers. However, since the isomerization rate constant fall-off and deuterium isotope effect are fairly insensitive to modest changes in these frequencies they give substantially the same agreement for these quantities as those of Rabinovitch and co-workers. Table 6 gives the final frequencies for the isotopic complexes. For comparison, the corresponding molecule frequencies are also included.

2. Isomerization Rate Constant and Fall-off

The complex models described in the preceding section were used to calculate the rate constant k for isomerization of CH_3NC as a function of pressure at each of the three temperatures of the investigations from the RRKM expression (Equation 43, p. 73). Input data for the calculation are: The reaction path multiplicity, $\alpha = 3$ (pp 81-83); the moments of inertia of the molecule (Table 4, p. 78) and of the complex (Table 6, p. 90); frequencies of Table 7 give a summary of the input data for the calculations. FORTRAN programs for calculating the vibrational degeneracy of the complex, the density of energy states for the active

Table 6. Frequencies and moments of inertia of isotopic molecules and complexes of methyl isocyanide

CH_3NC			$^{13}CH_3NC$			$CH_3N^{13}C$		
Molecule	8/30 Complex	10/40 Complex	Molecule	8/30 Complex	10/40 Complex	Molecule	8/30 Complex	10/40 Complex
3017(2)	3011(2)	3011(2)	3004(2)	3003(2)	3002(2)	3017(2)	3011(2)	3011(2)
2970	2970	2970	2966	2966	2966	2970	2970	2970
2134	1963	1921	2134	1963	1921	2095	1936	1893
1480(2)	1480(2)	1480(2)	1478(2)	1478(2)	1478(2)	1480(2)	1480(2)	1480(2)
1342	1342	1342	1326	1326	1326	1341	1341	1341
1011(2)	1011(2)	1011(2)	1004(2)	1004(2)	1004(2)	1011(2)	1011(2)	1001(2)
910	637	546	897	628	538	902	631	539
274(2)	301	274	274(2)	301	274	272(2)	297	272

$I_A^+ = 10.45$
$I_B^+ = 35.94$
$I_C^+ = 43.19$

$I_A^+ = 10.46$
$I_B^+ = 37.06$
$I_C^+ = 44.32$

$I_A^+ = 10.64$
$I_B^+ = 36.95$
$I_C^+ = 44.38$

Table 7. Input data for calculation of RRKM rate constant

Quantity and Symbol		Value	Reference
Reaction path Muliplicity, α		3	pp. 77-81
Principal moments of inertia, I^*, I^+	molecule	see reference	Table 4, p. 78
	complex		Table 6, p. 90
Frequencies of CH_3NC molecule and complex ν^*, ν^+		see reference	Table 6, p. 90
High-pressure activation energy, E_a		38.35 Kcal/mole	p. 54
Kinetic Theory collision diameter, σ		4.5 Å	p. 82, Ref. 36
Molecular weight, CH_3NC, M		41.02655 g/mole	
Collisional deactivation probability λ		1.0	p. 82
Temperature T			

molecule, and for evaluation of the RRKM rate integral by Simpson's rule were written and tested using hand calculations (carried to 8 decimal figures), and analytical functions designed to have a form similar to the RRKM rate integrand, respectively. Calculations were carried out on the M.S.U. Control Data 3600 digital computer. Integration steps of 5 cm^{-1} were used for most of the calculations, and the integration was carried to an energy sufficiently high that the value of the high-pressure integral gave the complex vibrational partition function to better than 0.1%; an upper integration limit of 10,000 cm^{-1} was generally sufficient for the purpose.

Several comparisons with experiments can be made, the most important being the shape and positioning of the fall-off curve, log k/k_∞ *vs.* log P, as shown in Figure 10 at 226°C. Open circles represent the results of this study. Data of Schneider at 230.4°C are included for a comparison (solid points). The agreement at the other temperatures is comparable. Our data is not as extensive as those of Schneider, the main purpose of this investigation being the determination of the Carbon-13 isotope effect. The agreement between the present results and those of Schneider are considered satisfactory. The RRKM calculated fall-off curves for both the 8/30 and 10/40 model are practically identical and are both represented by the solid line in Figure 10. The agreement with experiment is not as good as claimed by Schneider[36], but is considered satisfactory.

Figure 10.

Comparison of Experimental Rate Constant with RRKM Calculation.

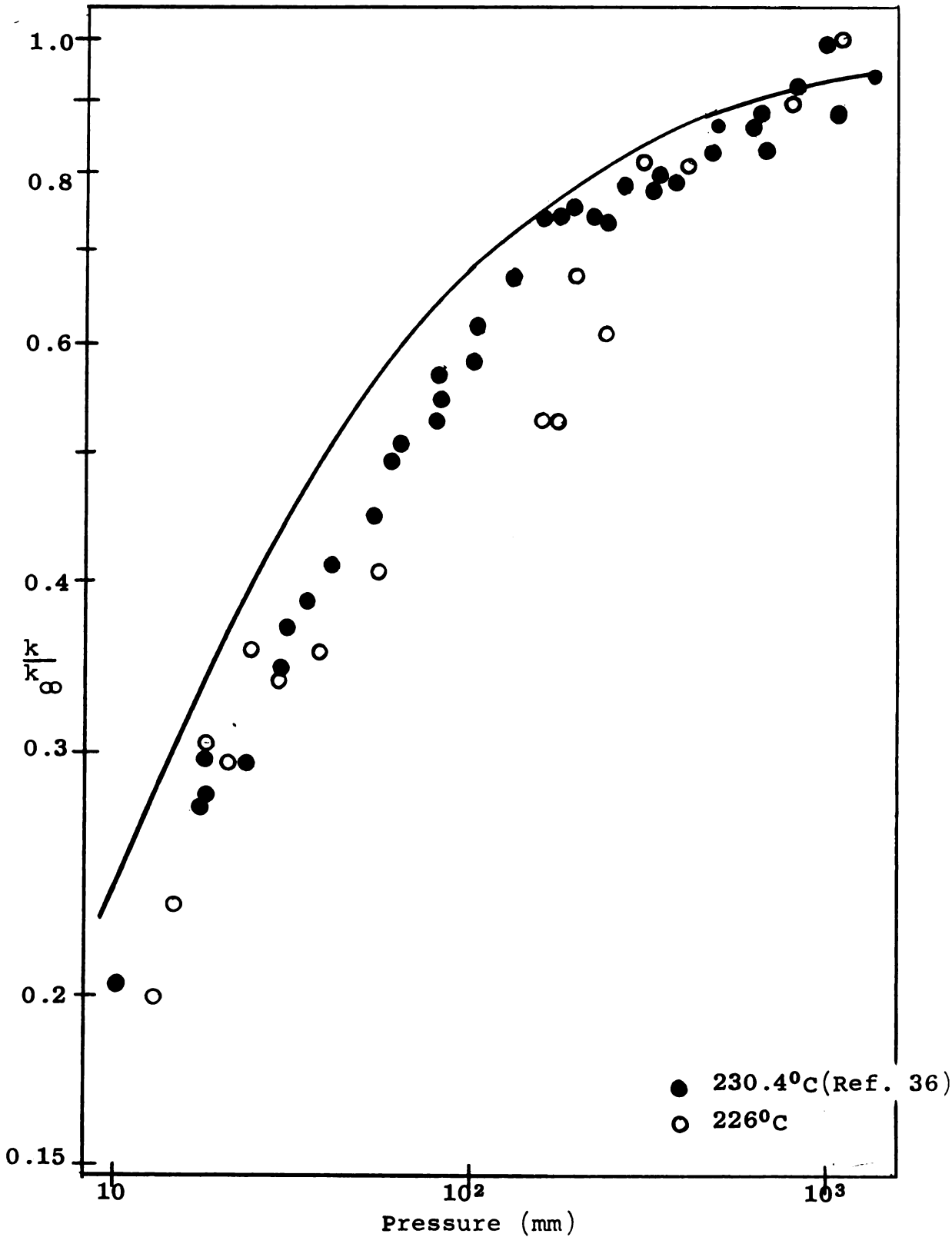

Figure 10.

The absolute positioning of the fall-off curve is dependent on the assumption of strong collisions, and extremely sensitive to the value of k_∞, which is obtained experimentally by extrapolating a plot of k^{-1} *vs.* $p^{-1/2}$ to $p = 0$, and is subject to considerable experimental error unless much more extensive high-pressure data are obtained.

The high-pressure rate constants obtained in this study, by Schneider[36], and the RRKM calculated values for both models are compared in Table 8. The agreement between the present work and that of Schneider is good. Both models give similar results in good agreement with experiment, although the agreement with the 8/30 model is somewhat better.

3. Carbon-13 Kinetic Isotope Effect

The rate constants for the isomerization of $^{13}CH_3NC$ (k_1) and $CH_3N^{13}C$ (k_2) were calculated as a function of pressure by RRKM in the same manner as just described for CH_3NC (k) by simply changing the input data in Table 7, p. 91 appropriate for the molecule in question. The isotope effects $r_1 = k/k_1$ and $r_2 = k/k_2$ were then calculated as a ratio of the appropriate rate constants at each pressure, and an "average" isotope effect r determined as described in Section A of this chapter.

The RRKM expression for an isotope effect k/k' at high pressures reduces to

Table 8. Comparison of limiting high-pressure rate constant

	10^5 k sec^{-1}		RRKM Calculated	
	This Study	Schneider[36]	8/30	10/40
213°C	25.0	---	23.0	28.4
226°C	75.0	92.5(230.4°C)	64.6	80.0
243.4°C	267	---	238	294
	Arrhenius Parameter			
E_a(Kcal/mole)	38.35	38.35	38.363	38.376
A (sec^{-1})	13.65	13.61	13.61	13.70

$$(k/k')_{\infty} = \left(\frac{I_r}{I'_r}\right)\left(\frac{Q'_v}{Q_v}\right)^{*}\left(\frac{Q_v}{Q'_v}\right)^{+} \exp\,(\Delta E_c/RT),$$

where the symbols have been previously defined. The $I_r Q^* Q^+$ term is always close to unity for carbon-13 isotope effects, and the magnitude of the calculated isotope effect is nearly determined by the value of ΔE_c. The calculated isotope effects r_1 and r_2 are thus dependent upon the assumption discussed earlier that $\Delta E_c \sim AE_a$ for both effects. However, as the value for C-13 isotope effects in unimolecular reactions is very close to 20 cal/mole observed for ΔE_a in this study, the assumption seems reasonable. Furthermore, changes in vibrational frequency pattern required to change ΔE_c also changes the $I_r Q^* Q^+$ ratio, so that the adjustment is not completely arbitrary. In all of the model calculations in this work, the prescriptions and limitations were adhered to rigidly and consistently, and changes made in the complex model for one molecule were carried through as corresponding changes for the other molecules. Thus, modest adjustments of this nature on the final frequency patterns would not effect the isotope fall-off or the magnitude of the effect unrealistically. Nevertheless, the calculated isotope effect is much more sensitive to details of the complex frequency patterns.

The comparison of the calculated average isotope effect $r = k/k'$ with experiment is shown in Figure 11 at 226°C. Comparable agreement is obtained at 243.4°C, and

Figure 11. Comparison of Experimental Isotope Effect with 8/30 and 10/40 Model RRKM Calculations.

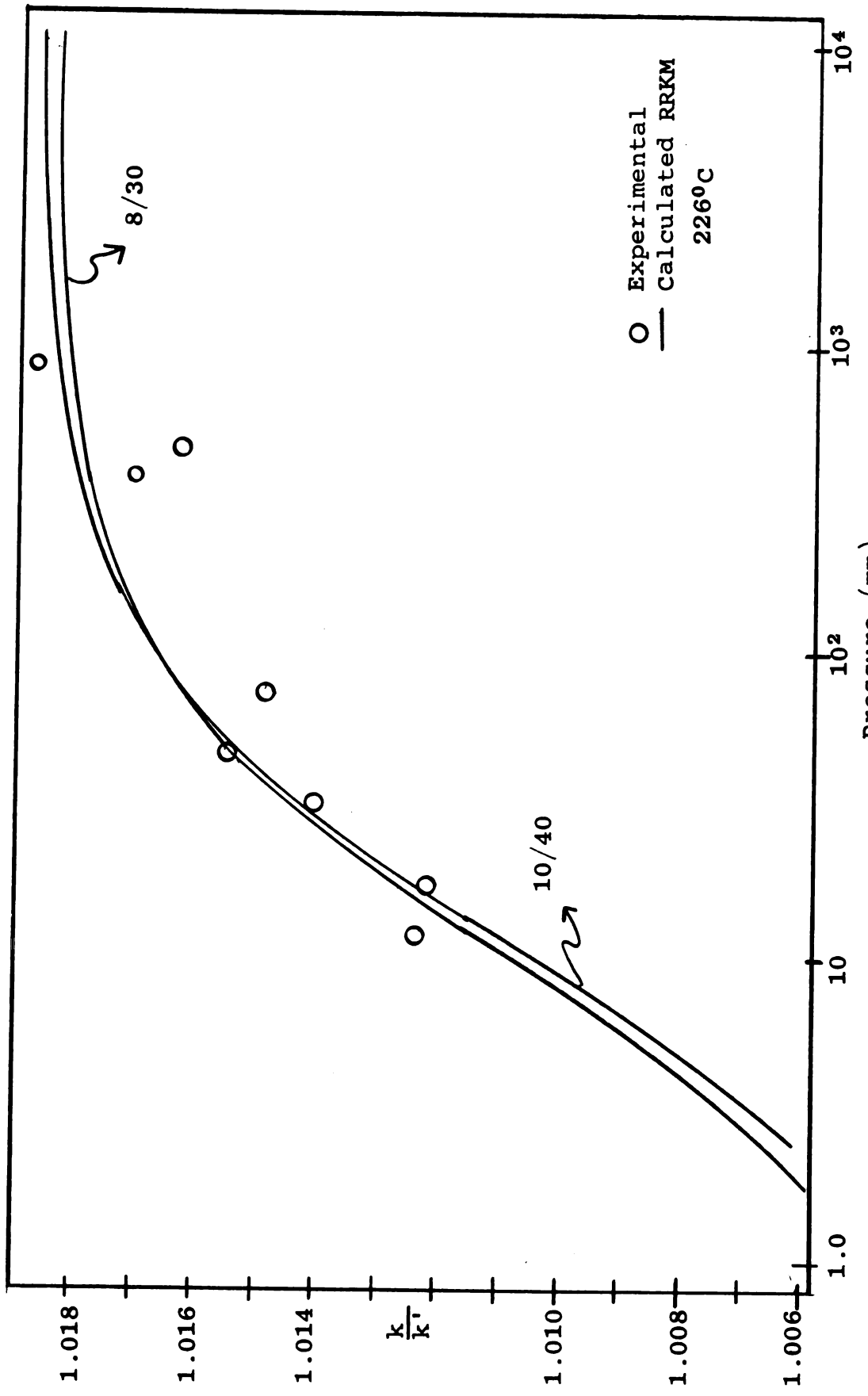
1.018
1.016
1.014
1.010
1.008
1.006
k/k'
1.0
10
10²
10³
10⁴
Pressure (mm)
8/30
10/40
O Experimental
— Calculated RRKM
226°C

Figure 11.

though only a few low-pressure results were obtained at 213°C, the present model is consistent with those results. The agreement generally is quite satisfactory over the pressure range studied. Plotting the data on a larger scale indicates clearly, however, that the 8/30 model fits slightly better than the 10/40 model. The main difference in the results of the two models, however, is between the high and extremely low pressure regions, where the 8/30 model predicts a smaller spread of extrenum values than does the 10/40 model. More data in these regions would be invaluable for refinement of the complex model.

The values of r_1, r_2, and the calculated average isotope effect r are compared at several pressures in Table 9. As can be seen from the results, the isotope effect arising from labeling the isonitrile carbon is substantially larger than that arising from labeling the methyl position. This effect was found in all of the models investigated; in fact, attempts to reverse this trend of changing the frequency patterns in the indicated direction as far as physically reasonable were unsuccessful. This differential effect is not entirely unexpected, since the vibrational analysis revealed that labeling the methyl carbon had a much less pronounced effect on the frequencies associated with the linear CNC submolecule than did isotope substitution at the isonitrile carbon.

The results substantiate the mechanism proposed by Rabinovitch and co-workers on the basis of the isomerization

Table 9. Calculated values of r_1, r_2, and average r at 226°C.

P(mm)	r_1		r_2		r	
	8/30	10/40	8/30	10/40	8/30	10/40
∞	1.01701	1.01610	1.01962	1.02105	1.01831_5	1.01857
10^4	1.01698	1.01606	1.01961	1.02104	1.01830	1.01855
10^3	1.01674	1.01577	1.01947	1.02088	1.01810_5	1.01833
10^2	1.01495	1.01361	1.01841	1.01968	1.01668	1.01665
10	1.00725	1.00627	1.01425	1.01482	1.01075	1.01055

rate constant fall-off and the deuterium isotope effect. The calculated carbon-13 isotope effect is more sensitive to the details of the complex frequency pattern than either of the other results, and the results indicate an increased "tightening" of the complex structure to that proposed previously; in particular, the results indicate that CNC bending frequency remaining as a "ring deformation" frequency of the complex is raised substantially from that in the molecule, a result to which the rate constant fall-off and deuterium isotope effect are insensitive. Confirmation of the new details of the complex vibrational frequency pattern will depend upon extending the range of investigation to both higher and lower pressures, and in particular to determining r_1 and/or r_2 separately in order to check the assumptions in the "averaging" process employed in this study. It is not expected that the temperature dependences of r_1 and r_2 will be found to be very different from one another, so that the results of this study should be valid at least in direction and approximately in magnitude.

BIBLIOGRAPHY

1. N. B. Slater, "Theory of Unimolecular Reactions", Ithaca, New York, Cornell Univ. Press, 1959.

2. F. A. Lindemann, Trans. Faraday Soc., 17, 598 (1922).

3. H. S. Johnston, "Gas Phase Reaction Rate Theory", The Ronald Press Company, New York, 1966.

4. C. N Hinshelwood, "The Kinetics of Chemical Change", Oxford Univ. Press, 1940.

5. O. K. Rice, and H. C. Ramsperger, J. Am. Chem. Soc., 49, 1617 (1927).

6. L. S. Kassel, "The Kinetics of Homogeneous Reactions", New York, The Chemical Catalog Co., Inc., 1932.

7. R. A. Marcus, J. Chem. Phys., 20, 359 (1952).

8. R. A. Marcus and O. K. Rice, J. Phys. and Colloid Chem., 55, 894 (1951).

9. R. L. Mills and H. S. Johnston, J. Am. Chem. Soc., 73, 938 (1951).

10. H. S. Johnston and R. L. Perrin, J. Am. Chem. Soc., 73, 4782 (1951).

11. A. F. Trotman-Dickenson, "Gas Kinetics", London, Butterworth Scientific Publications, 1955.

12. T. S. Chambers and G. B. Kistiakowsky, J. Am. Chem. Soc., 56, 399 (1934).

13. H. O. Pritchard, R. G. Sowden, and A. F. Trotman-Dickenson, Proc. Roy. Soc. (London), A217, 563(1953).

14. C. T. Genaux, F. Kern and W. D. Watters, J. Am. Chem. Soc., 73, 4497 (1951).

15. F. W. Schneider and B. S. Rabinovitch, J. Am. Chem. Soc., 84, 4215 (1962).

16. F. W. Schneider and B. S. Rabinovitch, J. Am. Chem. Soc., 85, 2365 (1963).

17. R. E. Weston, Jr., J. Chem. Phys., 26, 975 (1957).

18. A. T. Blades, Can. J. Chem., 39, 1401 (1961).

19. L. B. Sims and P. E. Yankwich, J. Phys. Chem., To be published.

20. L. B. Sims and P. E. Yankwich, In preparation.

21. F. J. Fletcher, B. S. Rabinovitch, K. W. Watkins, and D. J. Locker, J. Phys. Chem., 70, 2823 (1966).

22. S. Arrhenius, Z. physik, Chem., 4, 226 (1889).

23. H. S. Johnston, J. Chem. Phys., 20, 1103 (1952).

24. T. L. Hill, "Introduction to Statistical Thermodynamics", Reading, Mass., Addison-Wesley Publ. Co., Inc., 1960.

25. N. B. Slater, Phil. Trans. Roy. Soc., (London), A246, 57 (1953).

26. N. C. Hung and D. J. Wilson, J. Chem. Phys., 38, 828 (1963).

27. E. Thiele and D. J. Wilson, J. Chem. Phys., 35, 1256 (1961).

28. S. W. Benson, J. Chem. Phys., 34, 521 (1961).

29. O. K. Rice, J. Chem. Phys., 65, 1588 (1961).

30. S. Glasstone, K. J. Laidler, and H. Eyring, "The Theory of Rate Processes", New York, McGraw-Hill Book Co., 1941.

31. G. M. Wieder, Ph.D. Thesis, Polytechnic Institute of Brooklyn, 1960.

32. R. B. Bernstein, J. Phys. Chem., 56, 893 (1952).

33. B. S. Rabinovitch, D. W. Setser, and F. W. Schneider, can. J. Chem., 39, 2609 (1961).

34. R. A. Ogg, "The Experimental Basis for the Theory of Quasi-Unimolecular Reactions", J. Chem. Phys., 7, 753 (1939).

35. G. H. Kohlmaier and B. S. Rabinovitch, "Kinetics of the Thermal Isomerization of p-Tolyl Isocyanide", J. Phys. Chem., 63, 1793 (1959).

36. F. W. Schneider, Ph.D. Thesis, Univ. of Washington, 1962.

37. A. Gautier, Ann. Chim. Phys., 17, 215 (1869).

38. L. B. Sims, Ph.D. Thesis, Univ. of Illinois, 1967.

39. B. S. Rabinovitch, P. W. Gilderson, and A. T. Blades, J. Am. Chem. Soc., 86, 2994 (1964).

40. P. E. Yankwich and J. Y. Tong, J. Phys. Chem., 61, 540 (1957).

41. J. Bigeleisen and T. L. Allen, J. Chem. Phys., 19, 760 (1951).

42. E. B. Wilson, Jr., J. C. Decuis, P. C. Cross, "Molecular Vibrations", McGraw-Hill Book Company, Inc., New York, 1955.

43. G. Herzberg, "Infrared and Raman Spectra of Polyatomic Molecules," D. Van Norstrand Company, Inc., New York, 1947.

44. M. Kessler, H. Ring, R. Trambarula and W. Gordy, Phys. Rev., 79, 54 (1950).

45. H. Gilman, Editor, "Organic Chemistry, An Advanced Treatise", John Wiley and Sons, Inc., New York, 1943.

46. L. Pauling, "The Nature of the Chemical Bond", Cornell Univ. Press, Ithaca, New York, 1960.

47. J. H. Schachtschneider, Tech. Rept. No. 263-63, Shell Development Co., Emeryville, California.

48. M. E. K. Pillai and F. F. Cleveland, J. Mol. Spec., 5, 212 (1960).

49. R. A. Marcus, J. Chem. Phys., 43, 1598 (1965).

50. D. M. Bishop and K. J. Laidler, J. Chem. Phys., 42, 1688 (1965).

51. S. W. Benson, "The Foundations of Chemical Kinetics", McGraw-Hill Book Company, Inc., New York, 1960.

52. G. Z. Whitten and B. S. Rabinovitch, J. Chem. Phys., 38, 2466 (1963).

53. W. Kaplan, "Advanced Calculus", Addison-Wesley Publishing Company, Inc., 1952

54. A. Murray, III, and D. L. Williams, "Organic Synthesis with Isotopes", Interscience Publishers, Inc., New York, 1958.

APPENDIX

Studies Involving Labeled Methyl Isocyanide $^{13}CH_3NC$

Labeled methyl isocyanide ($^{13}CH_3NC$) was prepared from labeled barium carbonate $Ba^{13}CO_3$, 55 atom percent in a four step reaction sequence as follows[54]:

Step I. Preparation of $^{13}CO_2$:

$$Ba^{13}CO_3 + {}_2HClO_4 \longrightarrow Ba(ClO_4)_2 + H_2O + {}^{13}CO_2$$

Twelve and one-half milliliters of 70% $HClO_4$ was slowly added to a frozen mixture of 3.25 grams of $Ba^{13}CO_3$ in 6 ml of H_2O. The mixture was allowed to warm slowly and the resulting CO_2 was collected in a trap. The CO_2 was separated from the water and other products and purified by standard vacuum techniques.

Step II. Preparation of $^{13}CH_3OH$:

a) $4\ {}^{13}CO_2 + 3\ LiAlH_4 \xrightarrow{ROH} LiAl(O^{13}CH_3)_4 + 2\ LiAlO_2$

where ROH = diethylcarbitol(diethylene glycol diethyl ether).

b) $LiAl(O^{13}CH_3)_4 + {}_4R'OH \longrightarrow LiAl(OR')_4 + {}^{13}CH_3OH$

where R'OH = butyl carbitol(diethylene glycol, mono butyl ether).

The $^{13}CO_2$ obtained in Step I was slowly added to a frozen mixture of 1.8 grams of $LiAlH_4$ dissolved in 190 ml of diethyl carbitol. After all the CO_2 was adsorbed the mixture was allowed to come to room temperature and 30 grams

of butyl carbitol added slowly. After refluxing at 70°C for 2 hours, the $^{13}CH_3OH$ was distilled into a trap at -196°C. Impurities were removed by vacuum distillation from a salt bath at -20°C.

Step III. Preparation of $^{13}CH_3I$:

$$^{13}CH_3OH + HI \longrightarrow {}^{13}CH_3I + H_2O$$

The $^{13}CH_3OH$ obtained from Step II was transferred to a heavy wall glass reactor and cooled with liquid N_2. Twenty-five milliliters of HI (density = 1.7 g/ml) was added and the mixture heated to 90° for 2 hours. The product was purified by passage through a drying train of soda lime and P_2O_5 and collected in a sample bulb at -196°C.

Step IV. Preparation of $^{13}CH_3NC$:

a) $^{13}CH_3I + 2AgCN \longrightarrow {}^{13}CH_3NC \cdot AgCN + AgI$

b) $^{13}CH_3NC \cdot AgCN + KCN \longrightarrow CH_3NC + Ag(CN)_2^- + K^+ + I^-$

Labeled methyl isocyanide ($^{13}CH_3NC$) was prepared as described in Chapter III.

The $^{13}CH_3NC$ (55.8% label in methyl position was mixed with normal CH_3NC (natural abundance label in both positions) so that the final labeling in methyl position was about 3% since isotope-ratio mass spectrometer used in this study is limited to a maximum $^{13}CO_2/CO_2$ ratio of 10%, the signal/noise ratio increases rapidly with isotopic content of the carbon dioxide introduced.

The labeled methyl isocyanide was reacted, analyzed,

combusted, and the resulting CO_2 prepared for mass spectrometric analysis exactly as described for normal methyl isocyanide in Chapter III. The mass spectrometric results were, however, of such poor quality for the runs with labeled reactant that no useful results were obtained. No explanation of the poor operation of the mass spectometer for these samples is evident; however, similar difficulties have been encountered with enriched materials before by the mass spectrometer laboratory at the University of Illinois.